INTERNATIONAL JOURNAL OF
Plasticity

PERGAMON International Journal of Plasticity 15 (1999) 319–351

Strong discontinuities and continuum plasticity models: the strong discontinuity approach

J. Oliver*, M. Cervera, O. Manzoli

E.T.S. Enginyers de Camins, Canals i Ports, Technical University of Catalonia, Modul C-1, Campus Nord UPC, Gran Capita s/n, 08034 Barcelona, Spain

Received in final revised version 15 October 1998

Abstract

The paper presents the *Strong Discontinuity Approach* for the analysis and simulation of strong discontinuities in solids using continuum plasticity models. Kinematics of weak and strong discontinuities are discussed, and a regularized kinematic state of discontinuity is proposed as a mean to model the formation of a strong discontinuity as the collapsed state of a weak discontinuity (with a characteristic bandwidth) induced by a bifurcation of the stress–strain field, which propagates in the solid domain. The analysis of the conditions to induce the bifurcation provides a critical value for the bandwidth at the onset of the weak discontinuity and the direction of propagation. Then a variable bandwidth model is proposed to characterize the transition between the weak and strong discontinuity regimes. Several aspects related to the continuum and, their associated, discrete constitutive equations, the expended power in the formation of the discontinuity and relevant computational details related to the finite element simulations are also discussed. Finally, some representative numerical simulations are shown to illustrate the proposed approach.

1. Introduction

Strong discontinuities are understood here as solutions of the quasi-static solid mechanics problem exhibiting jumps in the displacement field across a material line (in 2D problems) or a material surface (in general 3D problems) which from now on will be named the *discontinuity line or surface*. The corresponding strains, involving material gradients of the displacements, are then unbounded at the discontinuity line or surface and remain bounded in the rest of the body.

*Corresponding author.

0749-6419/99/$—see front matter
PII: S0749-6419(98)00073-4

The strong discontinuity problem can be regarded as a limit case of the *strain localization* one, which has been object of intensive research in the last two decades (Rots et al., 1985; Ortiz et al., 1987; Ortiz and Quigley, 1991; de Borst et al., 1993; Lee et al., 1995), and where the formation of *weak discontinuities*, characterized by continuous displacements but discontinuous strains which concentrate or intensify into a band of finite width, is considered. As the width of the localization band tends to zero and the value of the strains jump tends to infinity the concept of strong discontinuity is recovered.

Plasticity models have been often analyzed in the context of strain localization and related topics: the slip lines theory (Chakrabarty, 1987) for rigid–perfectly plastic models is a paradigm of the use of plasticity models to capture physical phenomena involving discontinuities; the observed shear bands in metals can also be explained by resorting to J2 plasticity models in the context of strain-localization theories and weak discontinuities (Needleman and Tvergard, 1992; Larsson et al., 1993), etc.

Regarding strong discontinuities and their modeling via plasticity models, the topic has been tackled by different authors in the last years. In one of the pioneering works (Simo et al., 1993) the strong discontinuity analysis was introduced as a tool to extract those features that make a standard continuum (stress–strain) plasticity model compatible with the discontinuous displacement field typical of strong discontinuities. This work was later continued in (Simo and Oliver, 1994; Oliver, 1995a; Oliver, 1996a,b; Armero and Garikipati, 1995,1996; Oliver et al., 1997,1998), where different aspects of the same topic were examined, as well as in (Larsson et al., 1996; Runesson et al., 1996) in a slightly (regularized) different manner.

This paper aims to clarify the following questions concerning the capture of strong discontinuities using plasticity models:

- Under what conditions typical elasto-plastic (infinitesimal strains based) continuum constitutive equations, once inserted in the standard quasi-static solid mechanics problem, induce strong discontinuities having physical meaning and keeping the boundary value problem well posed?[1]
- What is the link of the *strong discontinuity approach*, based on the use of continuum (stress-strain) models, with the *discrete* discontinuity *approach* which considers a non-linear fracture mechanics environment and uses stress vs displacement-jump constitutive equations to model the de-cohesive behaviour of the discontinuous interface (Hillerborg, 1985; Dvorkin et al., 1990; Lofti and Ching, 1995)?
- What is the role of the fracture energy concept in this context?
- What are the connections of the strong discontinuity approach to the *discontinuous failure* theories (Runesson and Mroz, 1989; Runesson et al., 1991; Ottosen and Runesson, 1991; Steinmann and William, 1994; Stein et al., 1995) aiming at the prediction of the bifurcations induced by continuum constitutive equations?

[1]In the rest of this paper, the option of modelling strong discontinuities via *continuum* constitutive equations will be referred to as the *strong discontinuity approach*.

Total or partial answers to these questions are given in the next sections. For the sake of simplicity two dimensional problems (plane strain and plane stress) are considered although the proposed methodology can be easily extended to the general 3D cases. The remainder of the paper is structured as follows: Section 2 deals with the kinematics of the discontinuous problem and different options are analyzed. In Section 3 the target family of elastoplastic constitutive equations is described and the corresponding B.V. problem is presented in Section 4. In Section 5 the bifurcation analysis of general plasticity models is sketched and some interesting results are kept to be recovered in subsequent sections. In Section 6 the strong discontinuity analysis is performed and crucial concepts as the strong discontinuity equation, the strong discontinuity conditions and the discrete consistent constitutive equation are derived. In Section 7 a variable bandwidth model is presented as a possible mechanism to link weak to strong discontinuities and to provide a transition between them. In Section 8 the expended power concept in the formation of a strong discontinuity is examined and the conditions for recovering the fracture energy concept as a material property are established. Some details regarding the finite element simulation in the previously defined context are then given in Section 9. Sections 10 and 11 are devoted to present some numerical simulations to validate the proposed approach. Finally, Section 12 closes the paper with final remarks.

2. Weak and strong discontinuities: kinematics

Let us consider a bidimensional body Ω whose material points are labeled as $\mathbf{x}$, and a material (fixed along time) line $\mathcal{S}$ in Ω, with normal $\mathbf{n}$ [see Fig. 1(a)], which from now on will be called the *discontinuity line*. Let us also consider an orthogonal system of curvilinear coordinates ξ and η such that $\mathcal{S}$ corresponds to the coordinate line $\xi = 0 (\mathcal{S} := \{\mathbf{x}(\xi, \eta) \in \Omega; \xi = 0\}$. Let us denote by $\{\hat{\mathbf{e}}_\xi, \hat{\mathbf{e}}_\eta\}$ the physical (orthonormal) base associated to that system of coordinates and let $r_\xi(\xi, \eta)$ and $r_\eta(\xi, \eta)$ be the corresponding scale factors such that $\mathrm{d}s_\xi = r_\xi \, d\xi$ and $\mathrm{d}s_\eta = r_\eta \mathrm{d}\eta$, where $\mathrm{d}s_\xi$ and $\mathrm{d}s_\eta$ are, respectively, differential arc lengths along the coordinate lines ξ and η. We shall also consider the lines $\mathcal{S}^+$ and $\mathcal{S}^-$ which coincide with the coordinate lines $\xi = \xi^+$ and $\xi = \xi^-$, respectively, enclosing a *discontinuity band*, $\Omega^h := \{\mathbf{x}(\xi, \eta); \xi \in [\xi^-, \xi^+]\}$, whose representative width $h(\eta)$, from now on named *the bandwidth*, is taken as $h(\eta) = r_\xi(0, \eta)(\xi^+ - \xi^-)$. Let us finally define Ω^+ and Ω^- as the regions of $\Omega \backslash \Omega^h$ pointed to by $\mathbf{n}$ and $-\mathbf{n}$, respectively [see Fig. 1(a)] so that $\Omega = \Omega^+ \cup \Omega^- \cap \Omega^h$.

2.1. Kinematic state of weak discontinuity

Let us consider the displacement field $\mathbf{u}$ defined, in rate form, in Ω by:

$$\dot{\mathbf{u}}(\mathbf{x}, t) = \dot{\bar{\mathbf{u}}}(\mathbf{x}, t) + H_{\Omega^h}(\mathbf{x}, t)[\![\dot{\mathbf{u}}]\!](\mathbf{x}, t) \tag{1}$$

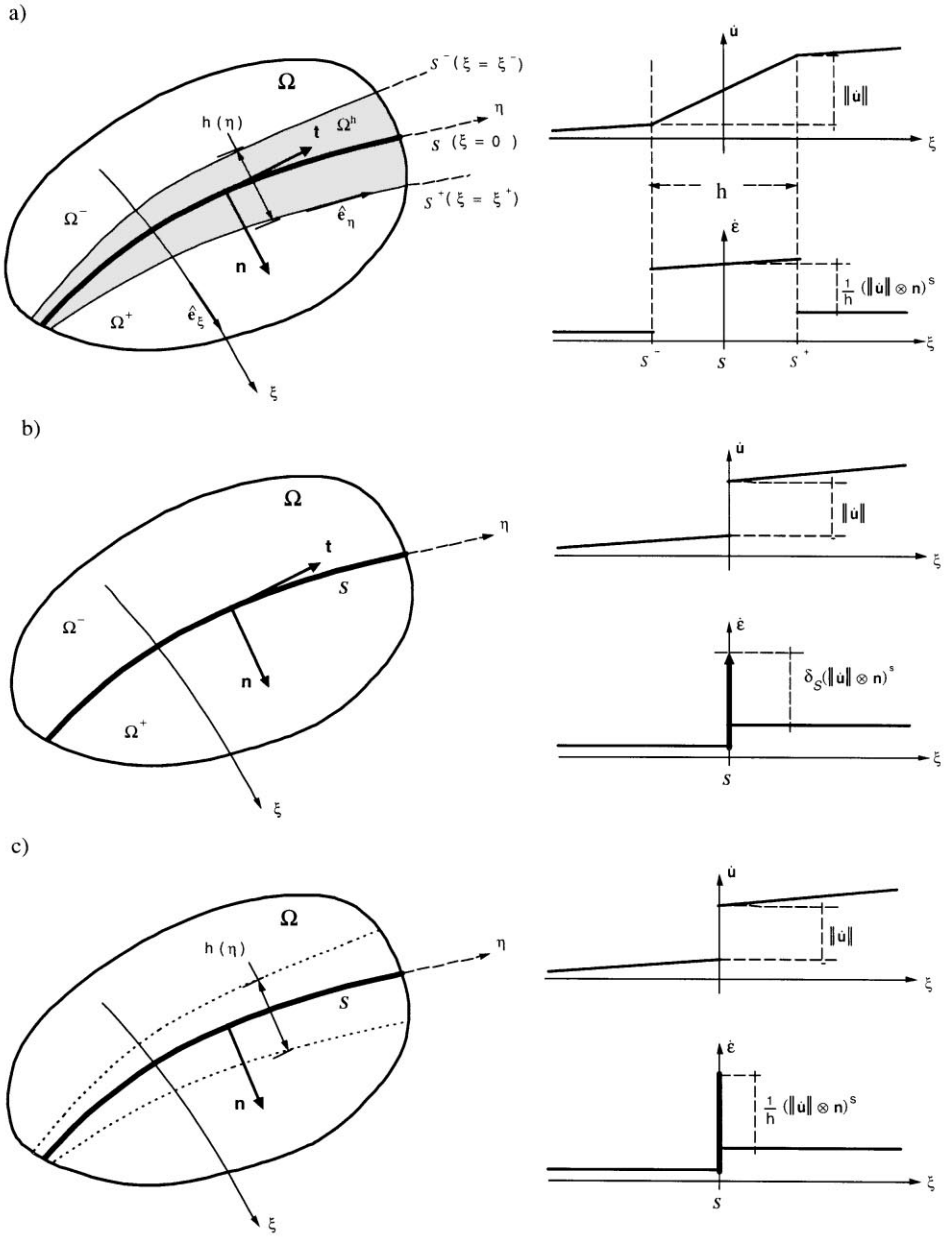

Fig. 1. Kinematics: (a) kinematic state of weak discontinuity; (b) kinematic state of strong discontinuity; (c) regularized kinematic state of discontinuity.

where t stands for the time, and $\dot{(\cdot)}$ stands for the time derivative of $(\cdot)$, $\bar{\mathbf{u}}(\mathbf{x}, t)$ and $[\![\mathbf{u}]\!](\mathbf{x}, t)$ are continuous $\mathcal{C}^0$ displacement fields and $H_{\Omega^h}(\mathbf{x}, t)$, from now on named the *unit ramp function*, is also a *continuous* function in Ω defined by:

$$H_{\Omega^h} = \begin{cases} 0 & \mathbf{x} \in \Omega^- \\ 1 & \mathbf{x} \in \Omega^+ \\ \dfrac{\xi - \xi^-}{\xi^+ - \xi^-} & \mathbf{x} \in \Omega^h \end{cases} \tag{2}$$

Clearly H_{Ω^h} exhibits a unit jump, as difference from its values at $\mathcal{S}^+$ and $\mathcal{S}^-$ for the same coordinate line ξ ($[\![H_{\Omega^h}]\!] = H_{\Omega^h}(\xi^+, \eta) - H_{\Omega^h}(\xi^-, \eta) = 1 \,\forall \eta$). From the definition of H_{Ω^h} in Eq. (2) the corresponding gradient can be computed as:

$$\begin{aligned} \nabla H_{\Omega^h} &= \frac{1}{r_\xi}\frac{\partial H_{\Omega^h}}{\partial \xi}\hat{\mathbf{e}}_\xi + \frac{1}{r_n}\frac{\partial H_{\Omega^h}}{\partial \eta}\hat{\mathbf{e}}_\eta = \mu_{\Omega^h}\frac{1}{h_\xi}\hat{\mathbf{e}}_\xi \\ h_\xi(\xi, \eta) &= r_\xi(\xi, \eta)(\xi^+ - \xi^-) \\ h_\xi(0, \eta) &= r_\xi(0, \eta)(\xi^+ - \xi^-) = h(\eta) \end{aligned} \tag{3}$$

where μ_{Ω^h} is a collocation function placed on Ω^h ($\mu_{\Omega^h} = 1$ if $\mathbf{x} \in \Omega^h$ and $\mu_{\Omega^h} = 0$ otherwise). From Eqs. (1) and (3) the kinematically compatible rate of strain $\dot{\boldsymbol{\epsilon}}$ can be computed as:

$$\dot{\boldsymbol{\epsilon}}(\mathbf{x}, t) = \nabla^s \dot{\mathbf{u}} = \underbrace{\nabla^s \dot{\bar{\mathbf{u}}} + H_{\Omega^h} \nabla^s [\![\dot{\mathbf{u}}]\!]}_{\dot{\bar{\boldsymbol{\epsilon}}}\,\text{(continuous)}} + \underbrace{\mu_{\Omega^h}\frac{1}{h_\xi}([\![\dot{\mathbf{u}}]\!] \otimes \hat{\mathbf{e}}_\xi)^s}_{[\![\dot{\boldsymbol{\epsilon}}]\!]\,\text{(discontinuous)}} \tag{4}$$

where superscript $(\cdot)^s$ stands for the symmetric part of $(\cdot)$. Eq. (4) states that the rate of strain field $\dot{\boldsymbol{\epsilon}}$ is the sum of a regular (continuous) part, $\dot{\bar{\boldsymbol{\epsilon}}}(\mathbf{x}, t)$, plus a discontinuous part, $[\![\dot{\boldsymbol{\epsilon}}]\!](\mathbf{x}, t)$, which exhibits jumps in $\mathcal{S}^-$ and $\mathcal{S}^+$ [see Fig. 1(a)]. Eqs. (1) and (4) define what will be referred to as *kinematic state of weak discontinuity* which can be qualitatively characterized by *discontinuous, but bounded, (rate of) strain fields*.

2.2. Kinematic state of strong discontinuity

We can now define the *kinematic state of strong discontinuity* as the limit case of the one describing a weak discontinuity when the band Ω^h collapses to the discontinuity line $\mathcal{S}$ [see Fig. 1(b)]. In other words, when $\mathcal{S}^+$ and $\mathcal{S}^-$ simultaneously tend to $\mathcal{S}$ [that is, with some abuse in the notation, $\xi^+ \to 0$, $\xi^- \to 0$, $h(\eta) \to 0$, and, thus, $\Omega^h \to \mathcal{S}$ in Fig. 1(a)]. In this case the unit ramp function (2) becomes a step function $H_{\mathcal{S}}(H_{\mathcal{S}}(\mathbf{x}) = 0 \,\forall \mathbf{x} \in \Omega^-$ and $H_{\mathcal{S}}(\mathbf{x}) = 1 \,\forall \mathbf{x} \in \Omega^+)$ and the rate of the displacement field (1) reads:

$$\dot{\mathbf{u}}(\mathbf{x}, t) = \dot{\bar{\mathbf{u}}}(\mathbf{x}, t) + H_{\mathcal{S}}[\![\dot{\mathbf{u}}]\!](\mathbf{x}, t) \tag{5}$$

the corresponding compatible rate of strain being:

$$\dot{\boldsymbol{\epsilon}}(\mathbf{x},t)=\nabla^s\dot{\mathbf{u}}=\underbrace{\nabla^s\dot{\tilde{\mathbf{u}}}+H_{\mathcal{S}}\nabla^s[\![\dot{\mathbf{u}}]\!]}_{\dot{\tilde{\boldsymbol{\epsilon}}}\,(\text{bounded})}+\underbrace{\delta_{\mathcal{S}}([\![\dot{\mathbf{u}}]\!]\otimes\mathbf{n})^s}_{[\![\dot{\boldsymbol{\epsilon}}]\!]\,(\text{unbounded})} \tag{6}$$

where $\delta_{\mathcal{S}}$ is a line Dirac's delta-function placed in $\mathcal{S}$. Now the (rate of) strain field (6) can be decomposed into $\dot{\tilde{\boldsymbol{\epsilon}}}$, exhibiting at most bounded discontinuities, and the unbounded counterpart $\delta_{\mathcal{S}}[\![\dot{\mathbf{u}}]\!]\otimes\mathbf{n})^{\mathcal{S}}$. Thus, by contrast with the weak discontinuity case, the strong discontinuity kinematic state can be characterized by the appearance of *unbounded (rate of) strain fields* along the discontinuity line S.

2.3. Regularized kinematic state of discontinuity

Finally, we consider a kinematic state defined by the following rates of displacement and strain fields:

$$\dot{\mathbf{u}}(\mathbf{x},t)=\dot{\tilde{\mathbf{u}}}(\mathbf{x},t)+H_{\mathcal{S}}[\![\dot{\mathbf{u}}]\!](\mathbf{x},t) \tag{7}$$

$$\dot{\boldsymbol{\epsilon}}(\mathbf{x},t)=\underbrace{\nabla^s\dot{\tilde{\mathbf{u}}}+H_{\mathcal{S}}\nabla^s[\![\dot{\mathbf{u}}]\!]}_{\dot{\tilde{\boldsymbol{\epsilon}}}\,(\text{regular})}+\underbrace{\mu_s\frac{1}{h(\eta)}([\![\dot{\mathbf{u}}]\!]\otimes\mathbf{n})^s}_{[\![\dot{\boldsymbol{\epsilon}}]\!]} \tag{8}$$

where $\mu_{\mathcal{S}}$ is a collocation function placed in $\mathcal{S}$ ($\mu_{\mathcal{S}}(\mathbf{x})=1\ \forall\mathbf{x}\in\mathcal{S}$, $\mu_{\mathcal{S}}(\mathbf{x})=0$ otherwise).

Comparison of Eqs. (7) and (8) with Eqs. (1) to (6) suggests the following remarks:

Remark 2.1. *The kinematic state defined by Eqs. (7) and (8) can be considered* representative *of a kinematic state of weak discontinuity of bandwidth $h(\eta)\neq 0$ (see Fig. 1(c)) in the following sense*:

- *The velocity field $\dot{\mathbf{u}}$ in Eq. (7) exhibits a jump of value $[\![\dot{\mathbf{u}}]\!]$ across the discontinuity line $\mathcal{S}$, whereas in Eq. (1) the jump appears between both sides ($\mathcal{S}^-$ and $\mathcal{S}^+$) of the discontinuity band Ω^h. If the bandwidth $h(\eta)$ is small with respect to the typical size of Ω, the former is representative of the later.*
- *The $\dot{\tilde{\boldsymbol{\epsilon}}}$ counterpart of the rate strain field (8) differs from the corresponding one in Eq. (4) in that a step function $H_{\mathcal{S}}$ is considered in the later instead of the unit ramp function H_{Ω^h} in the former. On the other hand the term $[\![\dot{\boldsymbol{\epsilon}}]\!]$ in Eq. (8) coincides with the value of $[\![\dot{\boldsymbol{\epsilon}}]\!]$ in Eq. (4) evaluated at the points of $\mathcal{S}$ [note that $h_\xi(0,\eta)=h(\eta)$, (see Eq. (3)) and that $\hat{\mathbf{e}}_\xi(0,\eta)=\mathbf{n}(\eta)$, (see Fig. 1(a)). In both cases they are representative of the corresponding values in Eq. (4) if the bandwidth $h(\eta)$ is relatively small in comparison to the typical size of Ω.*

Remark 2.2 *When the bandwidth $h(\eta)$ tends to zero the kinematic state defined by Eqs. (7) and (8) approaches a kinematic state of strong discontinuity as can be checked by comparison with Eqs. (5) and (6) and realizing that when $h(\eta)\to 0$, then $\mu_{\mathcal{S}}/h(\eta)\to\delta_{\mathcal{S}}$.*

Remark 2.3. *The rate of the strain field (8) is not kinematically compatible with the displacement field (7), in the sense that $\nabla^s\dot{\mathbf{u}}\neq\dot{\boldsymbol{\epsilon}}$, since $\nabla H_{\mathcal{S}}=\delta_{\mathcal{S}}\otimes\mathbf{n}\neq(\mu_{\mathcal{S}}/h(\eta))\otimes\mathbf{n}$. Compatibility is only approached when the bandwidth tends to zero as commented above.*

In the remainder of this paper we will consider Eqs. (7) and (8) as the description

of a kinematic state of weak discontinuity which approaches a kinematic state of strong discontinuity when the bandwidth h tends to zero.[2] Observe that, now, a kinematic state of weak discontinuity is characterized by a discontinuous (rate of) displacement field (7), jumping across a material line $\mathcal{S}$ and an incompatible, and discontinuous across $\mathcal{S}$, (rate of) strain field (8) whose amplitude along $\mathcal{S}$ is characterized by the bandwidth $h(\eta)$ [see Fig. 1(c)].

3. The elastoplastic constitutive equations

In the rest of this work we will consider the classical elasto-plastic constitutive equations which can be written as:

$$\begin{aligned}
&\dot{\boldsymbol{\sigma}} = \mathbf{C} : (\dot{\boldsymbol{\epsilon}} - \dot{\boldsymbol{\epsilon}}^p) \\
&\dot{\boldsymbol{\epsilon}}^p = \lambda \mathbf{m}^*(\boldsymbol{\sigma}) \\
&\dot{q} = -\lambda \mathcal{H}(q) \\
&\phi(\boldsymbol{\sigma}, q) = \hat{\phi}(\boldsymbol{\sigma}) + q - \sigma_y \\
&\mathbf{m}(\boldsymbol{\sigma}) = \partial_{\sigma} \phi(\boldsymbol{\sigma}, q) = \frac{\partial \hat{\phi}}{\partial \boldsymbol{\sigma}}
\end{aligned} \tag{9}$$

where $\boldsymbol{\sigma}$, $\boldsymbol{\epsilon}$ and $\boldsymbol{\epsilon}^p$ are the stress, total strain and plastic strain tensors, respectively, $\mathbf{C}$ is the elastic constitutive tensor ($\mathbf{C} = \hat{\lambda} \mathbf{1} \otimes \mathbf{1} + \mu \mathbf{I}$, $\mathbf{1}$ and $\mathbf{I}$ being, respectively, the rank-two and rank-four unit tensors and $\hat{\lambda}$ and μ the Lame's constants), q is the stress-like internal hardening variable, λ is the plastic multiplier, ϕ is the yield function, σ_y is the yield stress, $\mathcal{H}$ is the hardening/softening parameter, and $\mathbf{m}^*$ and $\mathbf{m}$ are, respectively, the plastic flow tensor and the normal to the yield surface $\Sigma_q := \{\boldsymbol{\sigma}\,;\, \phi(\boldsymbol{\sigma}, q) = 0\}$ ($\mathbf{m} = \mathbf{m}^*$ for associative plasticity). The model is supplemented by the loading–unloading (Kuhn–Tucker) and consistency conditions:

$$\begin{aligned}
&(\text{Kuhn}-\text{Tucker})\ \lambda \geqslant 0 \quad \phi(\boldsymbol{\sigma}, q) \leqslant 0 \quad \lambda \phi(\boldsymbol{\sigma}, q) = 0 \\
&(\text{Consistency})\ \lambda \quad \dot{\phi}(\boldsymbol{\sigma}, q) = 0 \text{ if } \phi(\boldsymbol{\sigma}, q) = 0
\end{aligned} \tag{10}$$

in such a way that the elastic and plastic behaviors are characterized by:

$$\begin{aligned}
&\phi < 0 \quad \Rightarrow \quad \lambda = 0 \quad \Rightarrow \quad \dot{\boldsymbol{\sigma}} = \mathbf{C} : \dot{\boldsymbol{\epsilon}}\ (\text{Elastic}) \\
&\phi = 0 \begin{cases} \dot{\phi} < 0 \quad \Rightarrow \quad \lambda = 0 \quad \Rightarrow \quad \dot{\boldsymbol{\sigma}} = \mathbf{C} : \dot{\boldsymbol{\epsilon}}\ (\text{Elastic unloading}) \\ \dot{\phi} = 0 \quad \Rightarrow \begin{cases} \lambda = 0\ (\dot{q} = 0) \quad \Rightarrow \quad \dot{\boldsymbol{\sigma}} = \mathbf{C} : \dot{\boldsymbol{\epsilon}}\ (\text{Neutral loading}) \\ \lambda > 0\ (\dot{q} \neq 0) \quad \Rightarrow \quad \dot{\boldsymbol{\sigma}} = \mathbf{C}^{ep} : \dot{\boldsymbol{\epsilon}}\ (\text{Plastic loading}) \end{cases} \end{cases}
\end{aligned} \tag{11}$$

[2] We could have started by *defining* a kinematic strain of weak discontinuity by means of Eqs. (7) and (8) instead of Eqs. (1) and (4). However, the introduction made here can help to identify the compatible kinematic state (7) and (8) as *representative* of the *compatible*, and consequently more familiar, kinematic state defined in Section 2.1 and Fig. 1 (a).

where the tangent elasto-plastic constitutive tensor, $\mathbf{C}^{ep}$, and the plastic multiplier λ can be computed as:

$$\mathbf{C}^{ep} = \mathbf{C} - \frac{\mathbf{C} : \mathbf{m}^* \otimes \mathbf{m} : \mathbf{C}}{\mathcal{H} + \mathbf{m}^* : \mathbf{C} : \mathbf{m}} \tag{12}$$

$$\lambda = \frac{\mathbf{m} : \mathbf{C} : \dot{\boldsymbol{\epsilon}}}{\mathcal{H} + \mathbf{m}^* : \mathbf{C} : \mathbf{m}} \tag{13}$$

4. The boundary value problem

Let us now consider the boundary of the body $\partial\Omega$ (see Fig. 2) with outward normal $\boldsymbol{\nu}$ and let $\Gamma_u \subset \partial\Omega$ and $\Gamma_\sigma \subset \partial\Omega$ ($\Gamma_u \cup \Gamma_\sigma = \partial\Omega$, $\Gamma_u \cap \Gamma_\sigma = \varnothing$) be parts of the boundary subjected to the usual essential and natural conditions, respectively. With the previously stated concepts in hand we can now formulate the boundary value problem as follows:

Find:

$$\begin{cases} \bar{\mathbf{u}}(\mathbf{x}, t) : \Omega \times \mathbb{I} \to \mathbb{R}^{n_{\text{dim}}} \\ [\![\mathbf{u}]\!](\mathbf{x}, t) : \Omega^+ \times \mathbb{I} \to \mathbb{R}^{n_{\text{dim}}} \end{cases} \tag{14}$$

such that $\mathbf{u}(\mathbf{x}, t) = \bar{\mathbf{u}}(\mathbf{x}, t) + H_s[\![\mathbf{u}]\!](\mathbf{x}, t)$ and

$$\begin{cases} \boldsymbol{\sigma}^-_{\Omega\setminus\mathcal{S}}(\mathbf{x}, t) : \Omega^- \times \mathbb{I} \to \mathbb{R}^{n_{\text{strs}}} \\ \boldsymbol{\sigma}^+_{\Omega\setminus\mathcal{S}}(\mathbf{x}, t) : \Omega^+ \times \mathbb{I} \to \mathbb{R}^{n_{\text{strs}}} \\ \boldsymbol{\sigma}_{\mathcal{S}}(\mathbf{x}, t) : \quad \mathcal{S} \times \mathbb{I} \to \mathbb{R}^{n_{\text{strs}}} \end{cases} \tag{15}$$

where $\mathbb{I}$ is the interval of interest, n_{dim} and n_{strs} are, respectively, the dimension of the body and the number of relevant stresses of the problem ($n_{\text{dim}} = 2$ and $n_{\text{strs}} = 4$ for 2D plane-strain cases and $n_{\text{dim}} = 2$ and $n_{\text{strs}} = 3$ for plane-stress cases)

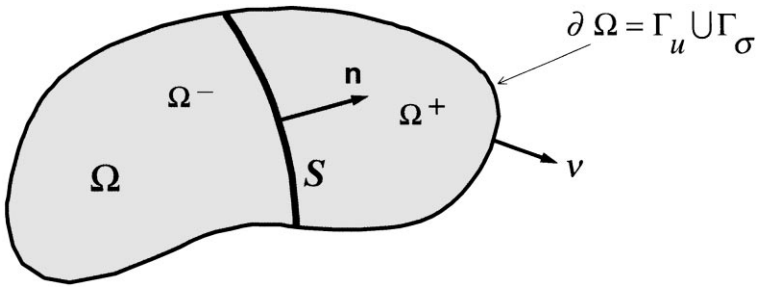

Fig. 2. Boundary value problem.

Such that:

$$\left.\begin{aligned}&\nabla\cdot\boldsymbol{\sigma}^{-}_{\Omega\setminus\mathcal{S}}+\mathbf{f}=\mathbf{0}\\&\nabla\cdot\boldsymbol{\sigma}^{+}_{\Omega\setminus\mathcal{S}}+\mathbf{f}=\mathbf{0}\end{aligned}\right\}\ \text{(equilibrium equation)}\tag{16}$$

$$\left.\begin{aligned}&\dot{\boldsymbol{\sigma}}^{+}_{\Omega\setminus\mathcal{S}}=\mathbb{C}^{+}_{\Omega\setminus\mathcal{S}}:\dot{\bar{\boldsymbol{\epsilon}}}\\&\dot{\boldsymbol{\sigma}}^{-}_{\Omega\setminus\mathcal{S}}=\mathbb{C}^{-}_{\Omega\setminus\mathcal{S}}:\dot{\bar{\boldsymbol{\epsilon}}}\\&\dot{\boldsymbol{\sigma}}_{\mathcal{S}}=\mathbb{C}_{\mathcal{S}}:[\dot{\bar{\boldsymbol{\epsilon}}}+\tfrac{1}{h}[\![\dot{\mathbf{u}}]\!]\otimes\mathbf{n}]^{\mathcal{S}}\end{aligned}\right\}\ \text{(constitutive equation)}\tag{17}$$

where $\mathbf{f}$ are the body forces, $\mathbb{C}$ stands for the tangent constitutive tensor ($\mathbb{C}=\mathbf{C}$ or $\mathbb{C}=\mathbf{C}^{ep}$ depending on the loading conditions (11)), and $\dot{\bar{\boldsymbol{\epsilon}}}=\nabla^{\mathcal{S}}\dot{\bar{\mathbf{u}}}+H_{\mathcal{S}}\nabla^{\mathcal{S}}[\![\dot{\mathbf{u}}]\!]$ is the regular (bounded) part of the rate of strain, subjected to the following:

Boundary conditions:

$$\left.\begin{aligned}&\mathbf{u}=\mathbf{u}^{*}(\mathbf{x},t)&&\mathbf{x}\in\Gamma_u\\&\boldsymbol{\sigma}_{\Omega\setminus\mathcal{S}}\cdot\boldsymbol{\nu}=\mathbf{t}^{*}(\mathbf{x},t)&&\mathbf{x}\in\Gamma_\sigma\\&\boldsymbol{\sigma}^{+}_{\Omega\setminus\mathcal{S}}\cdot\mathbf{n}=\boldsymbol{\sigma}^{-}_{\Omega\setminus\mathcal{S}}\cdot\mathbf{n}=\boldsymbol{\sigma}_{\mathcal{S}}\cdot\mathbf{n}&&\mathbf{x}\in\mathcal{S}\end{aligned}\right\}\begin{aligned}&\text{(prescribed displacements)}\\&\text{(prescribed tractions)}\\&\text{(traction continuity)}\end{aligned}\tag{18}$$

where $\mathbf{u}^{*}$ and $\mathbf{t}^{*}$ are the prescribed boundary displacements and tractions, respectively.

It is worth noting that Eq. $(18)_3$ states the continuity of the traction vector across the discontinuity line $\mathcal{S}$, in the sense that it takes the same value not only at both sides of $\mathcal{S}$ but also at the discontinuity line itself. As it will be shown in next sections this last condition provides an additional equation with respect to the regular continuum problem which allows the determination of the displacement jump $[\![\mathbf{u}]\!]$.

5. Bifurcation analysis. Onset and propagation of the discontinuity

We will now focus on the problem of the bifurcation of the stress-strain fields in the neighborhood of a given material point $\mathcal{P}$ in $\mathcal{S}$, constrained by the rate form of the traction continuity condition Eq. $(18)_3$:

$$\mathbf{n}\cdot\dot{\boldsymbol{\sigma}}_{\Omega/\mathcal{S}}=\mathbf{n}\cdot\dot{\boldsymbol{\sigma}}_{\mathcal{S}}\tag{19}$$

where the material character of $\mathcal{S}(\dot{\mathbf{n}}=0)$ has been considered.[3] The problem can be stated as follows: find under what conditions the stress–strain fields, continuous in a neighborhood of $\mathcal{P}(\boldsymbol{\sigma}_{\Omega/\mathcal{S}}=\boldsymbol{\sigma}_{\mathcal{S}},\ \boldsymbol{\epsilon}_{\Omega/\mathcal{S}}=\boldsymbol{\epsilon}_{\mathcal{S}})$ bifurcate into discontinuous rate of strain fields, $\dot{\boldsymbol{\epsilon}}_{\Omega/\mathcal{S}}=\dot{\bar{\boldsymbol{\epsilon}}}$ and $\dot{\boldsymbol{\epsilon}}_{\mathcal{S}}=\dot{\bar{\boldsymbol{\epsilon}}}+\frac{1}{h}([\![\dot{\mathbf{u}}]\!]\otimes\mathbf{n})^{\mathcal{S}}$, such that [see Eq. (17)]:

$$\left.\begin{aligned}&\dot{\boldsymbol{\sigma}}_{\Omega\setminus\mathcal{S}}=\mathbb{C}_{\Omega\setminus\mathcal{S}}:\dot{\bar{\boldsymbol{\epsilon}}}\\&\dot{\boldsymbol{\sigma}}_{\mathcal{S}}=\mathbb{C}_{\mathcal{S}}:[\dot{\bar{\boldsymbol{\epsilon}}}+\tfrac{1}{h}([\![\dot{\mathbf{u}}]\!]\otimes\mathbf{n})^{\mathcal{S}}]\end{aligned}\right.\tag{20}$$

subjected to condition (19). This problem has been widely analyzed in the context of the *failure analysis* of solids [see Runesson et al. (1991) for a complete analysis]

[3] No distinction is made here between $\dot{\boldsymbol{\sigma}}^{-}_{\Omega\setminus\mathcal{S}}$ and $\dot{\boldsymbol{\sigma}}^{+}_{\Omega\setminus\mathcal{S}}$. The reasoning following below is independent of the choice.

so it will only be sketched here. Substitution of Eq. (20) into (19) leads, after some algebraic manipulation, to:

$$\underbrace{(\mathbf{n}\cdot\mathbb{C}_s\cdot\mathbf{n})}_{\mathbf{Q}(\mathbf{n})}\cdot[\![\dot{\mathbf{u}}]\!] = h\,\mathbf{n}\cdot(\mathbb{C}_{\Omega\setminus\mathcal{S}} - \mathbb{C}_{\mathcal{S}}) : \dot{\bar{\boldsymbol{\varepsilon}}} \tag{21}$$

where $\mathbf{Q}(\mathbf{n})$ is the localization tensor (Steinmann and William, 1994). On the light of Eq. (21) we can now consider different possibilities for the onset of bifurcation:

(a) *The stress state* ($\boldsymbol{\sigma}_{\Omega\setminus\mathcal{S}} = \boldsymbol{\sigma}_{\mathcal{S}}$) *is elastic*. In this case $\mathbb{C}_{\Omega\setminus\mathcal{S}} = \mathbb{C}_{\mathcal{S}} = \mathbf{C}$, according to Eqs. (11) and (21) reads $\mathbf{Q}^e(\mathbf{n})\cdot[\![\dot{\mathbf{u}}]\!] = \mathbf{0}$, where $\mathbf{Q}^e = \mathbf{n}\cdot\mathbf{C}\cdot\mathbf{n}$ is the *elastic* acoustic tensor which is shown to be non singular ($\det(\mathbf{Q}^e) \neq 0$) (Runesson et al., 1991). Therefore, $[\![\dot{\mathbf{u}}]\!] = \mathbf{0}$ and bifurcation is precluded since then from Eq. (8) $\dot{\boldsymbol{\varepsilon}}_{\Omega\setminus\mathcal{S}} = \dot{\boldsymbol{\varepsilon}}_{\mathcal{S}} = \dot{\bar{\boldsymbol{\varepsilon}}}$ and $\dot{\boldsymbol{\sigma}}_{\Omega\setminus\mathcal{S}} = \dot{\boldsymbol{\sigma}}_{\mathcal{S}}$ from Eq. (20).

(b) *The stress state* ($\boldsymbol{\sigma}_{\Omega\setminus\mathcal{S}} = \boldsymbol{\sigma}_{\mathcal{S}}$) *is plastic*. Let us consider only bifurcations implying unloading or plastic neutral loading at $\Omega \setminus \mathcal{S}$ and loading at $\mathcal{S}$.[4] Thus, $\mathbb{C}_{\Omega\setminus\mathcal{S}} = \mathbf{C}$ and $\mathbb{C}_{\mathcal{S}} = \mathbf{C}^{ep}$ from Eq. (11). Now both possibilities (elastic unloading or plastic neutral loading in $\Omega \setminus \mathcal{S}$) should be explored. However, it can be shown (Runesson et al., 1991) that the second possibility is most critical (it is firstly reached in the context of decreasing values of the hardening parameter). Therefore, only plastic neutral loading in $\Omega \setminus \mathcal{S}$ and loading at $\mathcal{S}$ will be considered here. For this case Eq. (21) can be rewritten as:

$$\begin{aligned}\mathbf{n}\cdot\mathbf{C}^{ep}\cdot\mathbf{n}\cdot[\![\dot{\mathbf{u}}]\!] = h\,\mathbf{n}\cdot(\mathbf{C}-\mathbf{C}^{ep}) : \dot{\bar{\boldsymbol{\varepsilon}}} &= h\,\mathbf{n}\cdot\frac{\mathbf{C}:\mathbf{m}^*\otimes\mathbf{m}:\mathbf{C}:\dot{\bar{\boldsymbol{\varepsilon}}}}{\mathcal{H}+\mathbf{m}^*:\mathbf{C}:\mathbf{m}} \\ &= \lambda_{\Omega\setminus\mathcal{S}}\,h\,\mathbf{n}\cdot\mathbf{C}:\mathbf{m}^*\end{aligned} \tag{22}$$

where the structure of $\mathbf{C}^{ep}$ in Eq. (12) and the value of the plastic multiplier $\lambda_{\Omega\setminus\mathcal{S}}$ in Eq. (13) have been considered. Since plastic neutral loading is characterized by a null plastic multiplier ($\lambda_{\Omega/\mathcal{S}} = 0$) Eq. (22) finally reads:

$$\mathbf{Q}^{ep}\cdot[\![\dot{\mathbf{u}}]\!] = 0 \tag{23}$$

where $\mathbf{Q}^{ep} = \mathbf{n}\cdot\mathbf{C}^{ep}\cdot\mathbf{n}$ is the elasto-plastic localization tensor.

Eq. (23) establishes that, for the discontinuity to be initiated ($[\![\dot{\mathbf{u}}]\!] \neq \mathbf{0}$), the elasto-plastic localization tensor has to be singular, i.e.:

$$\det[\mathbf{Q}^{ep}(\mathbf{n},\mathcal{H})] = 0 \tag{24}$$

In Eq. (24) the dependence, for a given stress state, of the elasto-plastic localization tensor on the normal $\mathbf{n}$ and the hardening/softening parameter $\mathcal{H}$ is emphasized. Now, we can consider the set of values of $\mathcal{H}$ for which Eq. (23) as at least one solution for $\mathbf{n}$:

[4] Justification for this assumption will be given in Section 6 (see footnote 8).

$$\mathcal{G} = \left\{ \mathcal{H} \in \mathbb{R} | \; \exists \, \mathbf{n} \in \mathbb{R}^{n_{\text{ndim}}}; \; \| \, \mathbf{n} \, \| = 1; \; \det[\mathbf{Q}^{ep}(\mathbf{n}, \mathcal{H})] = 0 \right\} \tag{25}$$

If $\mathcal{G}$ is not empty we can consider the maximum value in this set as the critical one defining the bifurcation ($\mathcal{H}_{\text{crit}} = \max[\mathcal{H} \in \mathcal{G}]$). The corresponding solutions for $\mathbf{n}$ in Eq. (24) define the possible directions of propagation of the discontinuity, $\mathbf{n}_{\text{crit}}$, at point $\mathcal{P}$:

$$\mathbf{n}_{\text{crit}} \in \left\{ \mathbf{n} \in \mathbb{R}^{n_{n\,\text{dim}}}; \; \| \, \mathbf{n} \, \| = 1; \; \det[\mathbf{Q}^{ep}(\mathbf{n}, \mathcal{H}_{\text{crit}})] = 0 \right\} \tag{26}$$

For the considered 2D plane strain and plane stress problems explicit solutions can be given as follows. Let us consider the local orthonormal base $\{\mathbf{n}, \mathbf{t}, \hat{\mathbf{e}}_3\}$ where $\mathbf{n}$ and $\mathbf{t}$ are the normal and tangent vectors to $\mathcal{S}$ [see Fig. 1(b)] and $\hat{\mathbf{e}}_3 = \mathbf{n} \times \mathbf{t}$ is the out-of-plane unit vector and let m_{ij} and m^*_{ij}, $(i, j \in \{n, t, 3\})$ be the components of $\mathbf{m}$ and $\mathbf{m}^*$ in this local base. Let us also consider the unit vectors $\hat{\mathbf{e}}_1$ and $\hat{\mathbf{e}}_2$ corresponding to the in-plane principal directions of $\mathbf{m}$ and $\mathbf{m}^*$[5], and m_i and m^*_i $(i \in \{1, 2\}$, $m_1 > m_2, m^*_1 > m^*_2)$ the in-plane principal values, and $m_3 = m_{33}$ and $m^*_3 = m^*_{33}$ the corresponding out-of-plane principal values. Let finally θ be the inclination angle of $\mathbf{n}$ with respect to first principal direction $\hat{\mathbf{e}}_1$ such that $\mathbf{n} = \cos\theta \, \hat{\mathbf{e}}_1 + \sin\theta \, \hat{\mathbf{e}}_2$. The corresponding values of $\mathcal{H}_{\text{crit}}$ and θ_{crit} are presented in Table 1.[6]

Remark 5.1. *The preceding bifurcation analysis provides the conditions for the onset and progression of the discontinuity. Indeed, considering a discontinuity line $\mathcal{S}$ propagating across the body Ω, and a given material point $\mathcal{P}$, the first fulfillment at $\mathcal{P}$, for a certain time of the analysis $t_{\mathcal{P}}$, of the condition $\mathcal{H}(\mathcal{P}, t_{\mathcal{P}}) \leqslant \mathcal{H}_{\text{crit}}(\mathcal{P}, t_{\mathcal{P}})$ implies that: (a) the solution of the mechanical problem involves a jump in the rate of the displacement field at $\mathcal{P}$ (since $\mathcal{H} \in \mathcal{G}$ and, thus, $[\![\dot{\mathbf{u}}]\!]_P \neq \mathbf{0}$ from the bifurcation analysis) and, therefore, the stress and strain fields bifurcate; (b) the discontinuity line $\mathcal{S}$ has reached $\mathcal{P}$ at that time $t_{\mathcal{P}}$, and the normal $\mathbf{n}_{crit} = \mathbf{n}(\theta_{crit})$, provides the direction of progression of $\mathcal{S}$ from $\mathcal{P}$ towards other points in its neighbourhood. Moreover, since the discontinuity line is assumed a material (fixed) line, the obtained value for $\mathbf{n}(\mathcal{P}, t_{\mathcal{P}}) = \mathbf{n}_{crit}$ should be considered frozen beyond $t_{\mathcal{P}}$; (c) the bifurcation analysis has no sense at $\mathcal{P}$ for subsequent times, since the stress and strain fields will not remain continuous anymore.*

6. Strong discontinuity analysis

Substitution of Eqs. $(9)_1$ and $(9)_2$ into Eq. (8) allows to write the following evolution equation for the strains:

[5]It is implicitly assumed that the plastic flow vector $\mathbf{m}^*$ and the tensor normal to the yield surface $\mathbf{m}$ have the same principal directions. This is clearly true for associative plasticity ($\mathbf{m}^* = \mathbf{m}$) and also for the most frequently used yield and potential functions in 2D non associative plasticity (Lubliner, 1990).

[6]For practical purposes, the values of Table 1 are computed as follows: (1) The angle θ_{crit} (which is, in turn, determined from the values $\sin^2\theta_{\text{crit}}$ in the table, can be computed in terms of the principal values of $\mathbf{m}$ and $\mathbf{m}^*$; (2) then, the vector $\mathbf{n}$ and, therefore, the local base $\{\mathbf{n}, \mathbf{t}, \hat{\mathbf{e}}_3\}$ can be determined; (3) finally, the explicit values of $\mathcal{H}_{\text{crit}}$, in terms of the components of $\mathbf{m}$ and $\mathbf{m}^*$ in such local base, can be calculated.

Table 1
Results of the 2D bifurcation analysis for elasto-plastic constitutive models

Plane strain	
$\sin^2\theta_{\text{crit}}$	$-\dfrac{m_1(m_2^*+\nu m_{33}^*)+m_2(m_1^*-2m_2^*-\nu m_{33}^*)+\nu m_{33}(m_1^*-m_2^*)}{2(m_1-m_2)(m_1^*-m_2^*)}$
$\mathcal{H}_{\text{crit}}$	$-\dfrac{E}{(1-\nu)(1+\nu)}\{m_{tt}^*(m_{tt}+\nu m_{33})+m_{33}^*(m_{33}+\nu m_{tt})\}$
Plane stress	
$\sin^2\theta_{\text{crit}}$	$-\dfrac{m_2^*(m_1-m_2)+m_2(m_1^*-m_2^*)}{2(m_1-m_2)(m_1^*-m_2^*)}$
$\mathcal{H}_{\text{crit}}$	$-Em_{tt}^*m_{tt}$

$$\dot{\boldsymbol{\epsilon}}=\underbrace{\dot{\bar{\boldsymbol{\epsilon}}}}_{\text{bounded}}+\underbrace{\frac{\mu_{\mathcal{S}}}{h}(\llbracket\dot{\mathbf{u}}\rrbracket\otimes\mathbf{n})^{\mathcal{S}}}_{\text{unbounded for } h\to 0}=\underbrace{\mathbf{C}^{-1}:\dot{\boldsymbol{\sigma}}}_{\text{bounded}}+\lambda\mathbf{m}^*(\boldsymbol{\sigma}) \tag{27}$$

Let us examine under what conditions Eq. (27) is consistent with the appearance of a strong discontinuity characterized by $\llbracket\dot{\mathbf{u}}\rrbracket\neq\mathbf{0}$ and the limit case $h\to 0$.

We observe that the regular part of the strain $\dot{\bar{\boldsymbol{\epsilon}}}$ is bounded, by definition, and that the rate of the stress $\dot{\bar{\boldsymbol{\sigma}}}$ has also to remain bounded to keep its physical significance. Thus, for $\llbracket\dot{\mathbf{u}}\rrbracket$ not to vanish when the bandwidth h tends to zero the unbounded term $\frac{\mu_{\mathcal{S}}}{h}(\llbracket\dot{\mathbf{u}}\rrbracket\otimes\mathbf{n})^{\mathcal{S}}$ has to cancel out with some other unbounded term in the equation. In other words, the factor $\frac{\mu_{\mathcal{S}}}{h}$ has to appear in the last term of Eq. (27), the simplest choice being:[7]

$$\lambda=\mu_{\mathcal{S}}\frac{1}{h}\bar{\lambda}\Rightarrow\begin{cases}\lambda=0 & \forall\mathbf{x}\in\Omega\backslash\mathcal{S}\\ \lambda=\dfrac{1}{h}\bar{\lambda} & \forall\mathbf{x}\in\mathcal{S}\end{cases} \tag{28}$$

which states that elastic loading, unloading or plastic neutral loading [$\lambda=0$, see Eq. (11)] occurs in $\Omega\setminus\mathcal{S}$ whereas plastic loading occurs in $\mathcal{S}$.[8] We now observe that Eq. $(28)_2$ implies a particular structure of the hardening/softening parameter; substitution into Eq. $(9)_3$ leads to:

$$\mathcal{H}=-\frac{1}{\lambda}\dot{q}=h\underbrace{(-\frac{1}{\bar{\lambda}}\dot{q})}_{\bar{\mathcal{H}}}=h\bar{\mathcal{H}}\quad\forall\mathbf{x}\in S \tag{29}$$

Parameter $\bar{\mathcal{H}}$ in Eq. (29) will be referred to as the *intrinsic* or *discrete* hardening/softening parameter and it will be considered a material property.

Remark 6.1. *Eq. (28) states the localized character of the plastic flow once the discontinuity appears, i.e. once the discontinuity is triggered in a given point of $\mathcal{S}$, plastic*

[7] Eq. (28) has to be fulfilled *strictus sensus* only when $h\to 0$, that is, at the strong discontinuity regime. However, it will be held even in the weak discontinuity regime ($h\neq 0$) explored in Section 7.

[8] This justifies the choice made in Section 5 (see footnote 4).

strain rate is only allowed to develop at this point whereas its neighborhood at $\Omega \setminus S$ *experiences elastic loading or unloading* ($\lambda = 0$).

Remark 6.2. *Eq. (29) shows that as long as the strong discontinuity regime is approached* ($h \to 0$) *the hardening/softening parameter* $\mathcal{H}$ *tends to zero. Thus the strong discontinuity regime is only consistent with the part of the hardening/softening branch with null slope.*

We can now rewrite Eq. (27) restricted to points of $\mathcal{S}$ and considering Eqs. (28) and (29), as:

$$\underbrace{\dot{\bar{\boldsymbol{\varepsilon}}}}_{\text{bounded}} + \frac{1}{h}(\llbracket \dot{\mathbf{u}} \rrbracket \otimes \mathbf{n})^{\mathcal{S}} = \underbrace{\mathbf{C}^{-1} : \dot{\boldsymbol{\sigma}}}_{\text{bounded}} - \frac{1}{h}\frac{1}{\bar{\mathcal{H}}}\dot{q}\,\mathbf{m}^{*}(\boldsymbol{\sigma}) \quad \forall \mathbf{x} \in S \tag{30}$$

and we realize that as the strong discontinuity regime is approached ($h \to 0$) the unbounded terms have to cancel out each other leading to:

$$(\llbracket \dot{\mathbf{n}} \rrbracket \otimes \mathbf{n})^{S} = -\frac{1}{\bar{\mathcal{H}}}\dot{q}\ \ \mathbf{m}^{*}(\boldsymbol{\sigma}_{\mathcal{S}}) \tag{31}$$

6.1. Strong discontinuity condition

Eq. (31), that will be referred to as the *strong discontinuity equation*, establishes the evolution of the jump in the strong discontinuity regime and can be now specialized for the considered 2D problems.

6.1.1. Plane strain

Let us now focus on the 2D plane-strain problem considering, at any point of $\mathcal{S}$, the orthonormal base $\{\mathbf{n}, \mathbf{t}, \mathbf{e}_3\}$ defined in Section 5. In this base the (rate of) the displacement jump can be written as $\llbracket \dot{\mathbf{u}} \rrbracket = \llbracket \dot{u}_n \rrbracket \mathbf{n} + \llbracket \dot{u}_t \rrbracket \mathbf{t}$, where $\llbracket u_n \rrbracket$ and $\llbracket u_t \rrbracket$ are the normal and tangential components of the displacement jump at $\mathcal{S}$, and Eq. (31) reads, in terms of components:

$$\begin{bmatrix} \llbracket \dot{u}_n \rrbracket & \frac{1}{2}\llbracket \dot{u}_t \rrbracket & 0 \\ \frac{1}{2}\llbracket \dot{u}_t \rrbracket & 0 & 0 \\ 0 & 0 & 0 \end{bmatrix} = -\frac{1}{\bar{\mathcal{H}}}\dot{q} \begin{bmatrix} m^{*}_{nn} & m^{*}_{nt} & 0 \\ m^{*}_{nt} & m^{*}_{tt} & 0 \\ 0 & 0 & m^{*}_{33} \end{bmatrix}_{s} \tag{32}$$

where m^{*}_{ab}, $a, b \in \{n, t, 3\}$ are the components of the plastic flow tensor $\mathbf{m}^{*}$ in the chosen base. Eq. (32) can be regarded as a system of four non trivial equations with two unknowns ($\llbracket \dot{u}_n \rrbracket, \llbracket \dot{u}_t \rrbracket$) so that two equations involving only the flow tensor components m^{*}_{ij} can be extracted. They clearly are:

$$m^{*}_{tt_{\mathcal{S}}} = 0\ ;\ m^{*}_{33_{\mathcal{S}}} = 0 \tag{33}$$

6.1.2. Plane stress

Plane stress cases have to be studied in the projected space obtained by elimination of the out-of-plane components of the stresses and the strains. In this case Eq. (31) reads, in terms of components:

$$\begin{bmatrix} [\![\dot{u}_n]\!] & \frac{1}{2}[\![\dot{u}_t]\!] \\ \frac{1}{2}[\![\dot{u}_t]\!] & 0 \end{bmatrix} = -\frac{1}{\bar{\mathcal{H}}}\dot{q}\begin{bmatrix} m^*_{nn} & m^*_{nt} \\ m^*_{nt} & m^*_{tt} \end{bmatrix}_s \tag{34}$$

Here the system Eq. (34) includes three equations with the two unknowns $[\![\dot{u}_n]\!]$ and $[\![\dot{u}_t]\!]$ so that the following condition emerges:

$$m^*_{tt_S} = 0 \tag{35}$$

Eq. (33) and Eq. (35), which will be named *strong discontinuity conditions*, are clearly necessary conditions for the formation of a strong discontinuity. They are not, in general, fulfilled at the initial stages of the plastic flow and preclude, in most of cases, the formation of an strong discontinuity just at the bifurcation stage.

Remark 6.3. *It is illustrating to realize that substitution of conditions Eqs. (33) and (35) into the values of $\mathcal{H}_{crit}$ in Table 1 gives, both in the plane strain and plane stress cases, $\mathcal{H}_{crit} = 0$. This result can be justified as follows: (a) Eq. (21) holds at any stage of the problem since it comes from Eqs. (19) and (20) which hold for all the stages of the analysis; (b) the strong discontinuity regime is characterized by the limit case $h \to 0$ which implies that, for $[\![\dot{\mathbf{u}}]\!] \neq 0$ in Eq. (21) and loading cases ($\mathbb{C}_S = \mathbf{C}^{ep}_S$, then $det\left[(\mathbf{n}\cdot\boldsymbol{C}^{ep}_S\cdot\mathbf{n})\right] = det[\boldsymbol{Q}(\mathbf{n},\mathcal{H})] = 0$; (c) according to Eq. (29) at the strong discontinuity regime $h \to 0 \Rightarrow \mathcal{H} = 0$, whereby $det[\mathbf{Q}(\mathbf{n},\mathcal{H})]\,|_{\mathcal{H}=0} = 0$; (d) therefore, $\mathcal{H} = 0$ belongs to the set $\mathcal{G}$ [see Eq. (25)] of solutions for $\mathcal{H}$ of Eq. (24), which is given by the values $\mathcal{H} \leqslant \mathcal{H}_{crit}$. In other words: the solution $[\![\dot{\mathbf{u}}]\!]$ of the strong discontinuity problem lies in the null space of the perfectly plastic ($\mathcal{H} = 0$) localization tensor.*[9]

Remark 6.4. *In particular $\mathcal{H}_{crit} = 0$ is a necessary condition to induce a strong discontinuity. If that condition occurs at the bifurcation stage the bifurcation could take place under the form of a strong discontinuity. In the general case ($\mathcal{H}_{crit} \neq 0$) bifurcation will take place under the form of a weak discontinuity and the strong discontinuity conditions (33) or (35) must be induced in subsequent stages. In Section 7 a procedure to model the transition from the weak to the strong discontinuity regimes is proposed.*

Remark 6.5. *Bifurcation analysis of plastic models shows that, for the associative case ($\mathbf{m} = \mathbf{m}^*$) it occurs that $\mathcal{H}_{crit}(\sigma) \leqslant 0$. Moreover, for most of the stress states it is strictly $\mathcal{H}_{crit} < 0$ and, according to previous remarks, bifurcation can not take place in the form of a strong discontinuity. On the contrary, for non associative plasticity ($\mathbf{m} \neq \mathbf{m}^*$) it often happens that $\mathcal{H}_{crit}(\boldsymbol{\sigma}) > 0$, which could suggest that, since $\mathcal{H} = 0$ belongsto the set of admissible values $\mathcal{G}$ in Eq. (25), such value of the stresses is compatible with a bifurcation in the strong discontinuity fashion. However, the necessary strong discontinuity conditions Eqs. (33) or (35) and the subsequent necessary condition $\mathcal{H}_{crit}(\boldsymbol{\sigma}) = 0$ clearly preclude such possibility. Actually, this only refers to the bifurcation in a strong discontinuity fashion and not to the possibility of bifurcating under a weak discontinuity form and developing a strong discontinuity in subsequent stages.*

[9] This result was firstly stated in Simo et al. (1993).

6.2. Discrete constitutive equation

From Eqs. $(9)_4$ and $(9)_5$ and the consistency condition for loading cases ($\dot{\phi} = \mathbf{m} : \dot{\boldsymbol{\sigma}} + \dot{q} = 0$) the strong discontinuity Eq. (31) can be written:

$$(\llbracket \dot{\mathbf{u}} \rrbracket \otimes \mathbf{n})^S = \frac{1}{\bar{\mathcal{H}}} [\mathbf{m}(\boldsymbol{\sigma}_S) : \dot{\boldsymbol{\sigma}}(\boldsymbol{\sigma}_S)]\, \mathbf{m}^*(\boldsymbol{\sigma}_s) \tag{36}$$

which is regarded in conjunction with the traction continuity Eq. $(18)_3$

$$\mathbf{t}_{\Omega\setminus\mathcal{S}} = \boldsymbol{\sigma}_{\Omega\setminus\mathcal{S}} \cdot \mathbf{n} = \boldsymbol{\sigma}_{\mathcal{S}} \cdot \mathbf{n} \tag{37}$$

Eqs. (36) and (37) constitute, for any point of $\mathcal{S}$, a system of nine non trivial algebraic equations which states, for the general 3D case, the implicit dependence of nine unknowns (the six stress components $\boldsymbol{\sigma}_{\mathcal{S}}$ and the three jump components $\llbracket \mathbf{u} \rrbracket$) on the traction vector $\mathbf{t}_{\Omega\setminus\mathcal{S}}$:

$$\boldsymbol{\sigma}_{\mathcal{S}} = \mathcal{F}\big[\mathbf{t}_{\Omega\setminus\mathcal{S}}(t)\big] \tag{38}$$

$$\llbracket \mathbf{u} \rrbracket = \mathcal{I}\big[\mathbf{t}_{\Omega\setminus\mathcal{S}}(t)\big] \tag{39}$$

Remark 6.6. *Eq. (39) defines a discrete (traction- vs jump) constitutive equation at the interface $\mathcal{S}$. It is worth noting that it emerges naturally (consistently) from the continuum (stress-vs-strain) elasto-plastic constitutive equation described in Section 3 when the strong discontinuity kinematics is enforced. Thus, it is not strictly necessary neither to derive nor to make effective use of such discrete constitutive equation for modeling and numerical simulation purposes. In fact, the numerical solution scheme shown in Section 9 does not include the derivation of such equation and deals only with the standard elasto-plastic constitutive equation of Section 3 as the source constitutive equation.*

6.2.1. Example I: J2 (Von Mises) associative plasticity in plane strain

This case is characterized by the following expressions for the yield surface and the plastic flow tensor:

$$\begin{aligned} &\phi(\boldsymbol{\sigma}, q) = \bar{\sigma}(\boldsymbol{\sigma}) + q - \sigma_y \qquad \left(\bar{\sigma} = \sqrt{\tfrac{3}{2}} \parallel \mathbf{S} \parallel\right) \\ &\mathbf{m} = \mathbf{m}^* = \frac{\partial \phi}{\partial \boldsymbol{\sigma}} = \sqrt{\tfrac{3}{2}} \frac{\mathbf{S}}{\parallel \mathbf{S} \parallel} \end{aligned} \tag{40}$$

where $\mathbf{S}$ and $\bar{\sigma}$ stand for the deviatoric stresses and the effective stress, respectively. Specialization of Eqs. (32) and (36) for this case leads to:

$$\begin{bmatrix} \llbracket \dot{u}_n \rrbracket & \frac{1}{2}\llbracket \dot{u}_t \rrbracket & 0 \\ \frac{1}{2}\llbracket \dot{u}_t \rrbracket & 0 & 0 \\ 0 & 0 & 0 \end{bmatrix} = \frac{1}{\bar{\mathcal{H}}} \frac{3}{2} \left(\frac{\mathbf{S} : \dot{\mathbf{S}}}{\mathbf{S} : \mathbf{S}}\right)_{\mathcal{S}} \begin{bmatrix} S_{nn} & S_{nt} & 0 \\ S_{nt} & S_{tt} & 0 \\ 0 & 0 & S_{33} \end{bmatrix}_{\mathcal{S}} \tag{41}$$

From Eq. (41) it is immediately obtained that $S_{33_{\mathcal{S}}} = S_{tt_{\mathcal{S}}} = 0$ and then, due to the deviatoric character of $\mathbf{S}$ ($Tr\{\mathbf{S}\} = S_{nn} + S_{tt} + S_{33} = 0$), also $S_{nn_{\mathcal{S}}} = 0$. Therefore the

only non zero component of $\mathbf{S}$ is S_{nt} ($\mathbf{S} = S_{nt}[\mathbf{n} \otimes \mathbf{t}] + S_{nt}[\mathbf{t} \otimes \mathbf{n}]$) and then $(\mathbf{S} : \dot{\mathbf{S}})/(\mathbf{S} : \mathbf{S}) = \dot{S}_{nt}/S_{nt}$ so that finally we obtain from Eq. (41) the additional relationships $[\![\dot{u}_n]\!] = 0$ and $[\![\dot{u}_t]\!] = (3/\bar{\mathcal{H}})\dot{S}_{nt_\mathcal{S}}$. Hence, Eq. (41) is equivalent to the following system:

$$\begin{cases} \sigma_{nn_\mathcal{S}} = \sigma + S_{nn_\mathcal{S}} = \sigma & \sigma_{nt_\mathcal{S}} = S_{nt_\mathcal{S}} = \tau \\ \sigma_{tt_\mathcal{S}} = \sigma + S_{tt_\mathcal{S}} = \sigma & \sigma_{33_\mathcal{S}} = \sigma + S_{33_\mathcal{S}} = \sigma \end{cases} \tag{42}$$

$$\begin{cases} [\![\dot{u}_n]\!] = 0 \\ [\![\dot{u}_t]\!] = \dfrac{3}{\bar{\mathcal{H}}}\dot{\tau} \end{cases} \tag{43}$$

where σ (the mean stress) ant τ remain as unknowns. They can be determined by resorting to the two equations provided by the traction continuity condition Eq. (37) which for this 2D case read: $\sigma_{nn_\mathcal{S}} = \sigma_{nn_{\Omega\setminus\mathcal{S}}} = \sigma$ and $\sigma_{nt_\mathcal{S}} = \sigma_{nt_{\Omega\setminus\mathcal{S}}} = \tau$.

6.2.2. Example II: 2D Rankine associative plasticity.
The yield surface and flow tensor are now:

$$\begin{aligned} &\phi(\boldsymbol{\sigma}, q) = \sigma_1(\boldsymbol{\sigma}) + q - \sigma_y \\ &\mathbf{m} = \mathbf{m}^* = \hat{\mathbf{p}}_1 \otimes \hat{\mathbf{p}}_1 \end{aligned} \tag{44}$$

where σ_1 stands for the maximum in-plane principal stress ($\sigma_1 > \sigma_2$) and $\hat{\mathbf{p}}_1$ is the associated unit vector in the corresponding principal direction which is inclined the angle α with respect to $\mathbf{n}$ ($\hat{\mathbf{p}}_1 = \cos\alpha\,\mathbf{n} + \sin\alpha\,\mathbf{t}$). In the base $\{\mathbf{n}, \mathbf{t}, \mathbf{e_3}\}$ Eq. (36) now reads:

$$\begin{bmatrix} [\![\dot{u}_n]\!] & \frac{1}{2}[\![\dot{u}_t]\!] & 0 \\ \frac{1}{2}[\![\dot{u}_t]\!] & 0 & 0 \\ 0 & 0 & 0 \end{bmatrix} = \frac{1}{\bar{\mathcal{H}}}(\dot{\sigma}_1)_\mathcal{S} \begin{bmatrix} \cos^2\alpha & \sin\alpha\cos\alpha & 0 \\ \sin\alpha\cos\alpha & \sin^2\alpha & 0 \\ 0 & 0 & 0 \end{bmatrix} \tag{45}$$

where the result $\mathbf{m} : \dot{\boldsymbol{\sigma}} = \dot{\sigma}_1$ has been considered. From the component $(\cdot)_{22}$ of Eq. (45) we obtain $\sin^2\alpha = 0$ so that $\alpha = 0$ and $\mathbf{n} = \hat{\mathbf{p}}_1$. Thus, $\mathbf{n}$ is the first principal direction, then $\sigma_{nt_\mathcal{S}} = 0$ and the discontinuity line $\mathcal{S}$ develops perpendicularly to the first principal stress. Since $\sin\alpha = 0$ from component $(\cdot)_{12}$ of that equation we obtain $[\![\dot{u}_t]\!] = 0$ and, finally, $[\![\dot{u}_n]\!] = \frac{(\dot{\sigma}_1)_\mathcal{S}}{\bar{\mathcal{H}}}$ from component $(\cdot)_{11}$.

Therefore, Eq. (45) can be equivalently rewritten as:

$$\begin{cases} \sigma_{nn_\mathcal{S}} = \sigma_{1_\mathcal{S}} = \sigma \\ \sigma_{nt_\mathcal{S}} = 0 \end{cases} \tag{46}$$

$$\begin{cases} [\![\dot{u}_n]\!] = \dfrac{1}{\bar{\mathcal{H}}}\dot{\sigma} \\ [\![\dot{u}_t]\!] = 0 \end{cases} \tag{47}$$

where σ, the first principal stress, remains as an unknown that can be determined through the traction continuity condition $\sigma_{nn_S} = \sigma_{nn_{\Omega\setminus S}} = \sigma$.

Remark 6.7. *Eqs. (43) and (47) with $\sigma = \sigma_{nn_{\Omega\setminus S}}$ and $\tau = \sigma_{nt_{\Omega\setminus S}}$ are specializations of the general form Eq. (39) for the considered J2 (plane strain) and Rankine plasticity problems. Observe that the discrete constitutive Eq. (43) states that only the tangent component of the jump $[\![u_t]\!]$ can develop ($[\![u_n]\!] = 0$) so that with this type of J2 plasticity equations the generated strong discontinuity is a slip line (this result was also found in Simo et al., 1993; Oliver, 1996a; Armero and Garikipati, 1996). On the contrary Eq. (47) states that with Rankine-type plasticity models only Mode I (in terms of Fracture Mechanics) strong discontinuities can be modeled since the tangent component of the jump $[\![u_t]\!] = 0$. Obtaining such explicit forms of the discrete constitutive equations is not so straight-forward for other families of elastoplastic models. This makes specially relevant a methodology to approach strong discontinuities that does not require the explicit statement of such equations as pointed out in Remark 6.6.*

7. A variable bandwidth model

The bifurcation and strong discontinuity analyzes performed in Sections 6 and 7 above provide significant information about the mechanism to induce strong discontinuities. This can be summarized as follows:

- Bifurcation of the stress-strain fields is a necessary condition for the inception of a discontinuity in the displacement field. In the context of a variable hardening (or softening) law that bifurcation will take place, for a given material point, when the condition $\mathcal{H}(\boldsymbol{\sigma}) \leqslant \mathcal{H}_{\text{crit}}(\boldsymbol{\sigma})$ is fulfilled for the first time. In general $\mathcal{H}_{\text{crit}}(\boldsymbol{\sigma})$ will be non zero (Remark 6.5).
- Bifurcation will not, in general, produce the strong discontinuity. The necessary condition (to induce a strong discontinuity) $\mathcal{H}_{\text{crit}}(\boldsymbol{\sigma}) = 0$ will not, in general, be fulfilled at the bifurcation stage (Remarks 6.4 and 6.5) and bifurcation will take place under the form of a weak discontinuity.
- If the hardening/softening parameter $\mathcal{H}$ is expressed in terms of the *intrinsic hardening/softening parameter* $\bar{\mathcal{H}}$ (considered a material property) and the bandwidth h, according to Eq. (29) (i.e. $\mathcal{H} = h\bar{\mathcal{H}}$) then the bandwidth characterizing the weak discontinuity at the bifurcation will be given by $h_{\text{crit}} = \left(\mathcal{H}_{\text{crit}}/\bar{\mathcal{H}}\right) \neq 0$.

Therefore, if the aim of the model is to capture strong discontinuities an additional ingredient has to be introduced which provides: (a) the transition of the bandwidth from the value $h_{\text{crit}} \neq 0$, at the bifurcation, to the value $h = 0$, in a subsequent time and (b) the fulfillment of the strong discontinuity conditions Eqs. (33) or (35). In Fig. 3 what has been termed *variable bandwidth model* (Oliver et al., 1997 1998; Oliver, 1998) is sketched. It can be described in the following steps:

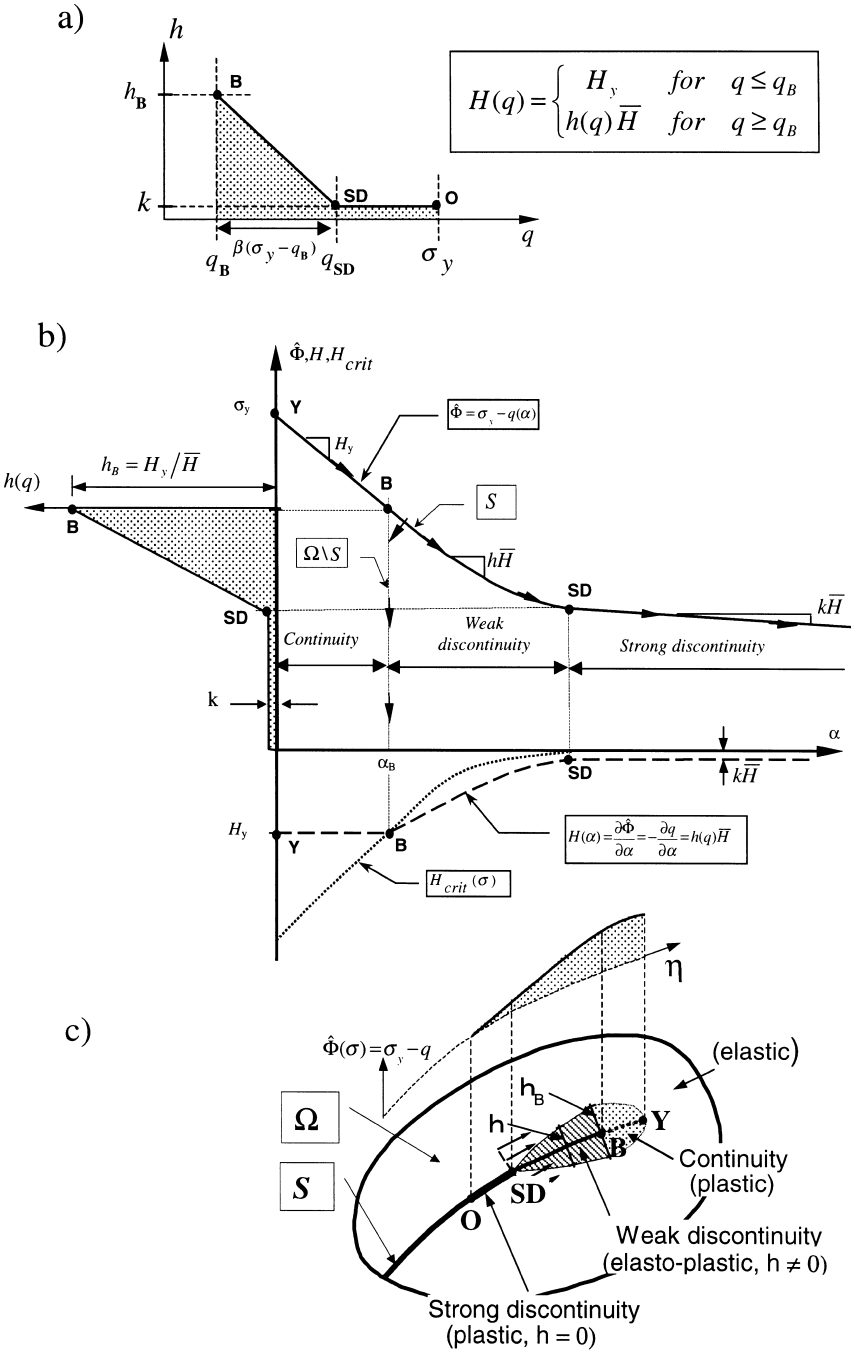

Fig. 3. Variable bandwidth model: (a) bandwidth law; (b) hardening/softening law and bandwidth evolution; (c) propagation of the discontinuity.

1. *Bandwidth law*. A certain variation of the bandwidth h, in terms of the stress-like variable $q \in [0, \sigma_y]$, is postulated [see Fig. 3a].[10] The bandwidth varies from $h = h_{\mathbf{B}}$, for a certain value $q_{\mathbf{B}}$ of the stress-like variable, which is attained at the *bifurcation point* **B**, to drop to $h = 0$ for another value (known and considered a model property)[11] $q_{\mathbf{SD}} \in [q_{\mathbf{B}}, \sigma_y]$, attained at the *strong discontinuity point* **SD**. In fact, for computational purposes the minimum value of h is limited to a very small regularization parameter k instead of zero (see Section 9 for more details). The value $h_{\mathbf{B}}$ is computed when the bifurcation is detected from the value of $\mathcal{H}_{\text{crit}}$ in Table 1 as $h_{\mathbf{B}} = \mathcal{H}_{\text{crit}}/\bar{\mathcal{H}}$.
2. *Hardening/softening parameters*. The model is considered ruled by two distinct hardening/softening $\mathcal{H}(q)$ parameters which relate the stress-like internal variable q and the hardening function $\hat{\phi} = \sigma_y - q$ to the strain-like internal variable α through:

$$-\frac{\partial q(\alpha)}{\partial \alpha} = \frac{\partial \hat{\phi}(\alpha)}{\partial \alpha} = \mathcal{H}(q) \tag{48}$$

   - Before the bifurcation ($q < q_{\mathbf{B}}$) the standard continuum hardening/softening law is characterized by the *continuum* hardening/softening parameter H_y[12] which is considered a material property [see Fig. 3a].
   - After the bifurcation ($q \in [q_{\mathbf{B}}, \sigma_y]$) the *discrete* hardening/softening parameter $\bar{\mathcal{H}}$ rules the cohesive/decohesive behavior at the discontinuous interface. However, Eq. (29) and the previously described bandwidth law provide the evolution of the corresponding continuum hardening/softening parameter as $\mathcal{H}(q) = h(q)\bar{\mathcal{H}}$. From this and from Eq. (48) the corresponding *continuum* hardening/softening law $q-\alpha$ can be readily obtained from integration of:

$$\frac{\partial q}{\partial \alpha} = -h(q)\bar{\mathcal{H}} \tag{49}$$

In Fig. 3b the corresponding $h(q)-q$, $\mathcal{H}-\alpha$ and $\hat{\phi}-\alpha$ curves are sketched. Observe that, according to Eq. (48), the curve $\mathcal{H}-\alpha$ supplies the slope of the hardening/softening curve $\hat{\phi}-\alpha$.

3. *Characteristic points: Continuous and Discontinuous regimes*. In Fig. 3(b) also a typical evolution of the values of $\mathcal{H}_{\text{crit}}$, obtained from Table 1, along the analysis

[10] In the figure the $h - q$ law has been plotted being linear. However other possibilities for the $h(q)$ curve (parabolic, exponential etc.) could have been alternatively considered.

[11] More precisely: for softening models what is considered a model property is the relative position of $q_{\mathbf{SD}}$ in the interval $[q_{\mathbf{B}}, \sigma_y]$, which is characterized by the value $\beta \in [0, 1]$ such that $q_{\mathbf{SD}} = q_{\mathbf{B}} + \beta(\sigma_y - q_{\mathbf{B}})$.

[12] For the sake of simplicity in Fig. 3 this parameter is considered constant and negative (strain softening) although more sophisticated non linear hardening or softening laws could have been considered.

is plotted. For a given material point yielding begins at point **Y** of Fig. 3(b), in which the hardening/softening parameter takes the value $\mathcal{H}_y$. While $\mathcal{H}_{\text{crit}} < \mathcal{H}_y$ bifurcation is precluded and the behavior is *continuous*. As soon as $\mathcal{H}_{\text{crit}} = \mathcal{H}_y$ the bifurcation point **B** is detected: the corresponding values of $\mathbf{n}(\theta_{\text{crit}})$ are computed from Table 1 which, once introduced in the rest of the model, warrant that bifurcation at point **B** takes place under the appropriate loading (at $\mathcal{S}$) and unloading (at $\Omega \setminus \mathcal{S}$) conditions [see Fig. 3(b)]. Also at this point the value $h_{\mathbf{B}} = \mathcal{H}_{\text{crit}}/\bar{\mathcal{H}}$, which states the initial value of the bandwidth law of Fig. 3(a), is computed. Since in general $h_{\mathbf{B}} \neq 0$, point **B** corresponds to the onset of a *weak discontinuity* whose bandwidth is enforced to decrease by the bandwidth law of Fig. 3(a) beyond this point. As soon as the value $q = q_{\mathbf{SD}}$ is attained at point **SD** and, according to the bandwidth law, $h = k \approx 0$ the strong discontinuity regime is reached and the strong discontinuity conditions Eq. (33) or (35) are naturally induced. Finally, beyond point **SD** the *strong discontinuity* regime develops keeping the bandwidth h and the continuum hardening/softening parameter $\mathcal{H}$ in a null (k-regularized) value.

Remark 7. *Since consistency with the results obtained from the bifurcation and strong discontinuity analyzes is kept along the process the obtained results warrant that: (a) bifurcation takes place under the appropriate loading–unloading conditions, thus not leading to a two materials approach (Oliver et al., 1997); and (b) the rate of the stresses remain bounded along the whole process keeping their physical significance.*

Translation of this variable bandwidth scheme in terms of the status of the material points of the body is finally sketched in Fig. 3(c), where a discontinuity line $\mathcal{S}$ that advances across the body Ω is represented. At a given time of the analysis most of the material points of the body Ω are in elastic state. Material points that are in plastic state define what in Non-linear Fracture Mechanics has been termed the *Fracture Process Zone* (Bazant and Oh, 1983): those points that lie in the **Y**−**B** branch of the curve in Fig. 3(b), define a continuous plastic (hardening or softening) zone. Points in the **B**−**SD** branch of the curve define the weak discontinuity part of the discontinuity line $\mathcal{S}$ to which a zone, whose bandwidth is defined by the corresponding bandwidth law $h(q)$, is associated in Fig. 3(c). Finally, material points remaining in the branch beyond point **SD**, in Fig. 3(b), define the strong discontinuity part of $\mathcal{S}$. In particular, point **O**, in Fig. 3(c), states the end of that segment of $\mathcal{S}$ whose material points have completely released stresses.

8. Expended power. Fracture energy

Let us now deal with the external mechanical power supplied to the body Ω of Fig. 2 along the deformation process. Neglecting the kinetic energy, and taking into account the existence of a displacement jump across the discontinuity line $\mathcal{S}$, the externally supplied mechanical power can be written as the sum of the contributions in Ω^+ and Ω^- ($\Omega^+ \cup \Omega^- = \Omega \setminus \mathcal{S}$):

$$
\begin{aligned}
\mathcal{P}^{\text{ext}} &= \int_{\Omega\setminus\mathcal{S}} \mathbf{f}\cdot\dot{\mathbf{u}}\,\mathrm{d}\Omega + \int_{\Gamma_u\cup\Gamma_\sigma} \boldsymbol{\nu}\cdot\boldsymbol{\sigma}\cdot\dot{\mathbf{u}}\,\mathrm{d}\Gamma \\
&= \int_{\Omega\setminus\mathcal{S}} \boldsymbol{\sigma}_{\Omega\setminus\mathcal{S}} : \dot{\bar{\boldsymbol{\varepsilon}}}\,\mathrm{d}\Omega + \int_{\mathcal{S}} \mathbf{n}\cdot\boldsymbol{\sigma}^{+}_{\Omega\setminus\mathcal{S}}\cdot\dot{\mathbf{u}}^{+}_{\Omega\setminus\mathcal{S}}\,\mathrm{d}\Gamma - \int_{\mathcal{S}} \mathbf{n}\cdot\boldsymbol{\sigma}^{-}_{\Omega\setminus\mathcal{S}}\cdot\dot{\mathbf{u}}^{-}_{\Omega\setminus\mathcal{S}}\,\mathrm{d}\Gamma \\
&= \int_{\Omega\setminus\mathcal{S}} \boldsymbol{\sigma}_{\Omega\setminus\mathcal{S}} : \dot{\bar{\boldsymbol{\varepsilon}}}\,\mathrm{d}\Omega + \int_{\mathcal{S}} \mathbf{n}\cdot\boldsymbol{\sigma}_{\mathcal{S}}\cdot\underbrace{(\dot{\mathbf{u}}^{+}_{\Omega\setminus\mathcal{S}} - \dot{\mathbf{u}}^{-}_{\Omega\setminus\mathcal{S}})}_{[\![\dot{\mathbf{u}}]\!]}\,\mathrm{d}\Gamma \\
&= \underbrace{\int_{\Omega\setminus\mathcal{S}} \boldsymbol{\sigma}_{\Omega\setminus\mathcal{S}} : \dot{\bar{\boldsymbol{\varepsilon}}}\,\mathrm{d}\Omega}_{\mathcal{P}^{\text{int}}_{\Omega\setminus\mathcal{S}}} + \underbrace{\int_{\mathcal{S}} \boldsymbol{\sigma}_{\mathcal{S}} : ([\![\dot{\mathbf{u}}]\!]\otimes\mathbf{n})^{s}\,\mathrm{d}\Gamma}_{\mathcal{P}^{\text{int}}_{\mathcal{S}}}
\end{aligned}
\tag{50}
$$

where the traction vector continuity condition $\left(\mathbf{n}\cdot\sigma^{+}_{\Omega\setminus\mathcal{S}} = \mathbf{n}\cdot\sigma^{-}_{\Omega\setminus\mathcal{S}} = \mathbf{n}\cdot\sigma_{\mathcal{S}}\right)$ has been considered. We observe in Eq. (50) that $\mathcal{P}^{\text{int}}_{\Omega\setminus\mathcal{S}}$ and $\mathcal{P}^{\text{int}}_{\mathcal{S}}$ are *volumetric* and *surface* counterparts of the supplied external power, respectively. Thus, we can understand $\mathcal{P}^{\text{int}}_{\mathcal{S}}$ as the part of the external power internally spent in the formation of the jump $[\![\dot{\mathbf{u}}]\!]$ at the discontinuity interface $\mathcal{S}$. Therefore, taking into account Eq. (30) we can write $\mathcal{P}^{\text{int}}_{\mathcal{S}}$, after some algebraic manipulation, as:

$$
\mathcal{P}^{\text{int}}_{\mathcal{S}} = \underbrace{\int_{\mathcal{S}} h\boldsymbol{\sigma}_{\mathcal{S}} : (\mathbf{C}^{-1} : \dot{\boldsymbol{\sigma}}_{\mathcal{S}} - \dot{\bar{\boldsymbol{\varepsilon}}})\mathrm{d}\Gamma}_{=O(h)} - \int_{\mathcal{S}} \frac{1}{\bar{\mathcal{H}}}\dot{q}\boldsymbol{\sigma}_{\mathcal{S}} : \mathbf{m}^{*}\mathrm{d}\Gamma \tag{51}
$$

We now observe that the first integral of the right-hand-side of Eq. (51) is bounded and tends to zero with the bandwidth h. Thus, if the bandwidth is small with respect to the representative size of Ω it can be neglected. Let us now specialize the problem to the cases fulfilling the following conditions:

1. The function $\hat{\phi}(\boldsymbol{\sigma})$ in Eq. $(9)_4$ is an homogeneous function (of degree one) of the stresses.[13] In this case, in virtue of Euler's theorem for homogeneous functions, it can be written:

$$
\partial_{\boldsymbol{\sigma}}\hat{\phi} : \boldsymbol{\sigma} = \hat{\phi}(\boldsymbol{\sigma}) \tag{52}
$$

2. Associative plasticity ($\mathbf{m}^{*} = \mathbf{m} = \partial_{\boldsymbol{\sigma}}\hat{\phi}$)
3. Strain-softening (which implies that q remains in the bounded interval $[0, \sigma_y]$)

We also observe that, for loading processes ($\lambda \neq 0$), Eq. $(10)_1$ implies that $\phi = 0$, and, thus, $\sigma_y - q = \hat{\phi} = \partial_{\boldsymbol{\sigma}}\hat{\phi} : \boldsymbol{\sigma} = \mathbf{m} : \boldsymbol{\sigma}$ [see Eqs. $(9)_4$, $(9)_5$ and (52)]. So that, finally, Eq. (51) can be written as:

[13] This is a requirement fulfilled by many usual yield functions [Von-Mises, Tresca, Mohr–Coulomb, Drucker Prager, Rankine, etc. (Khan, 1995).

$$\begin{aligned}\mathcal{P}_{\mathcal{S}}^{int} &= \int_{\mathcal{S}} \boldsymbol{\sigma}_{\mathcal{S}} : (\llbracket \dot{\mathbf{u}} \rrbracket \otimes \mathbf{n})^s \mathrm{d}\Gamma \\ &\simeq -\int_{\mathcal{S}} \frac{1}{\bar{\mathcal{H}}} \dot{q}\, \boldsymbol{\sigma}_{\mathcal{S}} : \mathbf{m} \mathrm{d}\Gamma = -\int_{\mathcal{S}} \frac{1}{\bar{\mathcal{H}}} \dot{q}\, (\sigma_y - q)\, \mathrm{d}\Gamma = \\ &= \int_{\mathcal{S}} \frac{\partial}{\partial t} \underbrace{\left[\frac{1}{2\bar{\mathcal{H}}} (\sigma_y - q)^2 \right]}_{\varphi(q)} \mathrm{d}\Gamma = \int_{\mathcal{S}} \frac{\partial}{\partial t} \varphi(q) \mathrm{d}\Gamma\end{aligned} \tag{53}$$

Let us now compute the energy $\mathcal{W}_{\mathcal{S}}$ spent at $\mathcal{S}$ along *any* loading process leading to the formation of a strong discontinuity. The *complete* loading process can be characterized by the evolution of the stress-like variable q ranging from $q = 0$ at the unloaded initial state ($t = 0$) to $q = \sigma_y$ at the final state ($t = t_\infty$) where the stresses are compleately released:

$$\mathcal{W}_{\mathcal{S}} = \int_0^{t_\infty} \mathcal{P}_{\mathcal{S}}^{int} \mathrm{d}t = \int_0^{t_\infty} \left[\int_{\mathcal{S}} \frac{\partial}{\partial t} \varphi(q) \mathrm{d}\Gamma \right] dt = \int_{\mathcal{S}} \underbrace{\left[\int_0^{t_\infty} \frac{\partial}{\partial t} \varphi(q) \mathrm{d}t \right]}_{G_f} \mathrm{d}\Gamma \tag{54}$$

The kernel of the last integral of Eq. (54) can be now identified as the energy spent, per unit of surface, in the formation of the strong discontinuity which, in the context of the non-linear fracture mechanics, is referred to as the *fracture energy* G_f. In view of Eqs. (53) and (54) it can be written:

$$G_f = \int_0^{t_\infty} \frac{\partial}{\partial t} \varphi(q) \mathrm{d}t = \int_{q=0}^{q=\sigma_y} \frac{\partial}{\partial q} \varphi(q) \mathrm{d}q = \varphi(\sigma_y) - \varphi(0) = -\frac{1}{2} \frac{\sigma_y^2}{\bar{\mathcal{H}}} \tag{55}$$

so that, finally, Eq. (55) can be solved for the intrinsic hardening/softening parameter, $\bar{\mathcal{H}}$, in terms of the *material properties* σ_y and G_f as:

$$\bar{\mathcal{H}} = -\frac{1}{2} \frac{\sigma_y^2}{G_f} \tag{56}$$

Remark 8.1. *Results (55) and (56) have been obtained for an arbitrary loading process. The material property character of the resulting fracture energy, lies crucially onto this fact since the value of G_f in Eq. (55) is independent of the loading process. This result, in turn, comes out directly from Eq. (53), namely: $\boldsymbol{\sigma}_{\mathcal{S}}$: $(\llbracket \dot{\mathbf{u}} \rrbracket \otimes \mathbf{n})^s$ is an exact time differential ($\boldsymbol{\sigma}_{\mathcal{S}} : (\llbracket \dot{\mathbf{u}} \rrbracket \otimes \mathbf{n})^s = \frac{\partial}{\partial t} \varphi(q)$). Notice that this is not a completely general result since it has been obtained under the conditions (a)–(c) above.*

Remark 8.2. *The existence of the fracture energy as a bounded and positive material property is then restricted to associative plasticity models with strain softening according to conditions (b) and (c). In fact, there is no intrinsic restriction for non-associative strain-hardening constitutive equations to induce strong discontinuities. In that case the intrinsic hardening/softening parameter $\bar{\mathcal{H}}$ would have to be positive*

according to the condition $\bar{\mathcal{H}} = (\mathcal{H}/h) > 0$. However, this scenario does not ensure neither the existence of the fracture energy, as a material property independent of the loading process, nor a bounded value for the energy $\mathcal{W}_{\mathcal{S}}$ in Eq. (54) (since in that case $q \in [0, -\infty]$). On the other hand, the positiveness of $\bar{\mathcal{H}}$ would lead to a cohesive (instead of decohesive) character of the resulting discrete constitutive equation at the interface.

9. Finite element simulation. Computational aspects

The ingredients of the approach presented above can now be considered for the numerical simulation of strong discontinuities, via finite elements. It was pointed out in Remark 6.6 that the discrete (stress-jump) constitutive Eq. (39) obtained from the strong discontinuity analysis is not in fact used for numerical simulation purposes but, on the contrary, it emerges naturally from the continuum stress-straincon-stitutive equation when the strong discontinuity kinematics is enforced. In consequence, a standard finite element code for 2D elasto-plastic analysis only needs some few modifications to implement the present model. Essentially these are:

- Standard C^0 finite elements have to be modified in order to make them able to capture jumps in the displacement field. In Oliver (1995b, 1996b) details about a family of such elements, which has proved very efficient, can be found. They are based in an enhancement of the strain field of the standard underlying element by adding a discontinuous incompatible mode for the displacements. Also an extra-integration point is considered where the specific kinematic and constitutive properties of the interface $\mathcal{S}$ are modeled (see Fig. 4).
- The standard elasto-plastic constitutive model has to be slightly modified to include the hardening/softening law Eq. (29).

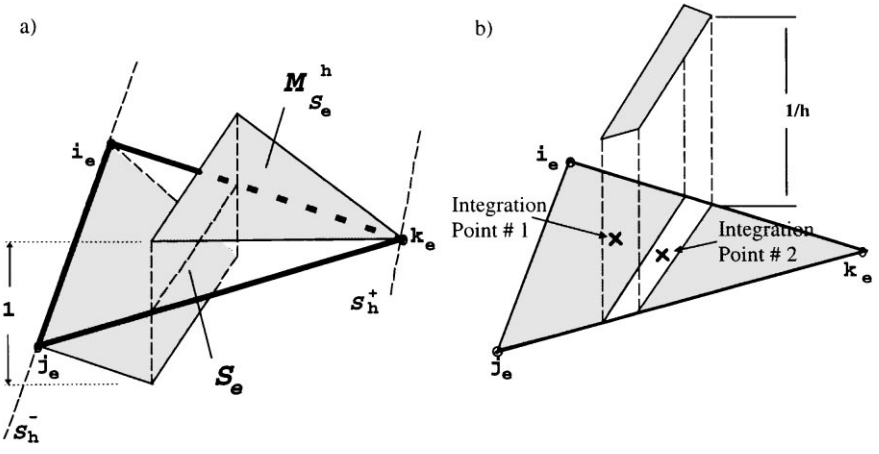

Fig. 4. Finite element with embedded discontinuity: (a) discontinuous shape function; (b) discontinuous strain field and additional sampling point.

- Computation of the bifurcation condition $\mathcal{H} < \mathcal{H}_{\text{crit}}$ and the corresponding direction of propagation of the discontinuity has to be included. For 2D cases results in Table 1 can be used. Also the bifurcation bandwidth of Eq. (48) and the bandwidth evolution of Eq. (49) have to be computed according to the values $\mathcal{H}_{\text{crit}}$ in Table 1.
- In a strain driven algorithm, Eq. (8) has to be numerically integrated to obtain the strain field at any given time of the analysis. In fact the rate of the strain field at $\mathcal{S}$:

$$\dot{\boldsymbol{\varepsilon}}_{\mathcal{S}} = \dot{\bar{\boldsymbol{\varepsilon}}} + \frac{1}{h(q)}(\dot{[\![\mathbf{u}]\!]} \otimes \mathbf{n})^{S} \tag{57}$$

cannot be analytically integrated due to the appearance of $h(q(\bar{\varepsilon}, [\![\mathbf{u}]\!]))$ which is given in Eq. (49). In the examples shown below the following mid-point rule (second order accuracy) has been used:

$$\begin{aligned} h_{t+\frac{\Delta t}{2}} &= \frac{1}{2}[\underbrace{h(\bar{\boldsymbol{\varepsilon}}_{t+\Delta t}, [\![\mathbf{u}]\!]_{t+\Delta t})}_{h_{t+\Delta t}} + \underbrace{h(\bar{\boldsymbol{\varepsilon}}_{t}, [\![\mathbf{u}]\!]_{t})}_{h_{t}}] \\ \boldsymbol{\epsilon}_{\mathcal{S}_{t+\Delta t}} &= \boldsymbol{\epsilon}_{\mathcal{S}_{t}} + \Delta\bar{\boldsymbol{\varepsilon}} + \frac{1}{h_{t+\frac{\Delta t}{2}}}(\Delta[\![\mathbf{u}]\!] \otimes \mathbf{n})^{s} \end{aligned} \tag{58}$$

where subscripts $(\cdot)_{t+\Delta t}$ and $(\cdot)_{t}$ refer to evaluation at the end of two consecutive time steps and $\Delta(\cdot) = (\cdot)_{t+\Delta t} - (\cdot)_{t}$ are the corresponding increments.

- In order to avoid ill-conditioning in Eq. (57) when $h \to 0$, the evolution of h given by Eq. (49) is limited to $h \in [h_{\text{crit}}, k]$ where $k > 0$ is a very small regularization parameter. Typically, k is taken about 10^{-2}–10^{-3} times the size of the finite element. In Oliver (1995a, 1996b) the objectivity (independence) of the results with respect to such regularization parameter is shown, provided it is small with respect to the typical finite element size.

10. A first illustrative example: uniaxial tension test

A very simple, but illustrative, example is now examined in order to assess the capacity of the approach to induce strong discontinuities and to reproduce the theoretical predictions of the strong discontinuity analysis (essentially, the discrete constitutive equation at the interface). A J2 (Von-Mises) model of associative plasticity is taken as target constitutive equation and the results are checked via an uniaxial tension test under plane strain conditions. In Fig. 5(a) the loading and geometrical features of the problem are presented. A linear bandwith law with $\beta = 0.15$ has been taken. Since the stress field is uniform, the discontinuity must be seeded somewhere; therefore, the lower left corner element of the unstructured finite

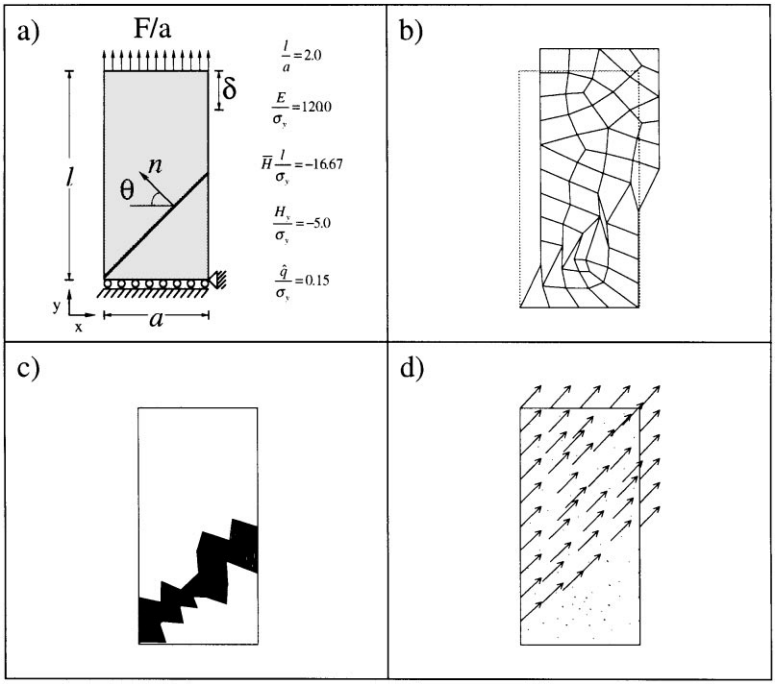

Fig. 5. Uniaxial tension test and J2 plasticity (plane strain).

element mesh of quadrilateral elements of Fig. 5(a) is chosen for this purpose. In Fig. 5(b) the deformed shape at the final stage of the analysis is shown. It can be checked there that the deformation corresponds to an almost rigid body motion of the upper part of the specimen slipping along a straight slip-line, which starts at the aforementioned element and crosses the band of elements highlighted in Fig. 5(c). In this figure the contours of the total displacements group in the patch of elements that capture the discontinuity[14] stating the sharp resolution of the jump. In Fig. 5(d) the slip-line deformation mode is emphasized by displaying the displacement vectors of the nodes of the finite element mesh.

In Fig. 6 the evolution of different variables of the problem is shown in a non-dimensional fashion. Figure 6(a)–(e) are obtained using a Poisson ratio $\nu = 0$ whereas Fig. 6(f) corresponds to different values of ν ($\nu = 0$ and $\nu = 0.5$).

Figure 6(a) shows the bandwidth evolution, h, at a certain element of the discontinuity path, in terms of the total displacement δ of Fig. 5(a). The relevant part of the curve is the one going from $h = h_B$, at the *bifurcation point* **B**, to $h = k = 10^{-3}l$ at the inception of the strong discontinuity, the *strong discontinuity point* **SD**.

[14] For post-processing purposes only displacements of the regular underlying elements are displayed. Displacements corresponding to the elemental discontinuous incompatible modes referred to in Section 9 are not displayed.

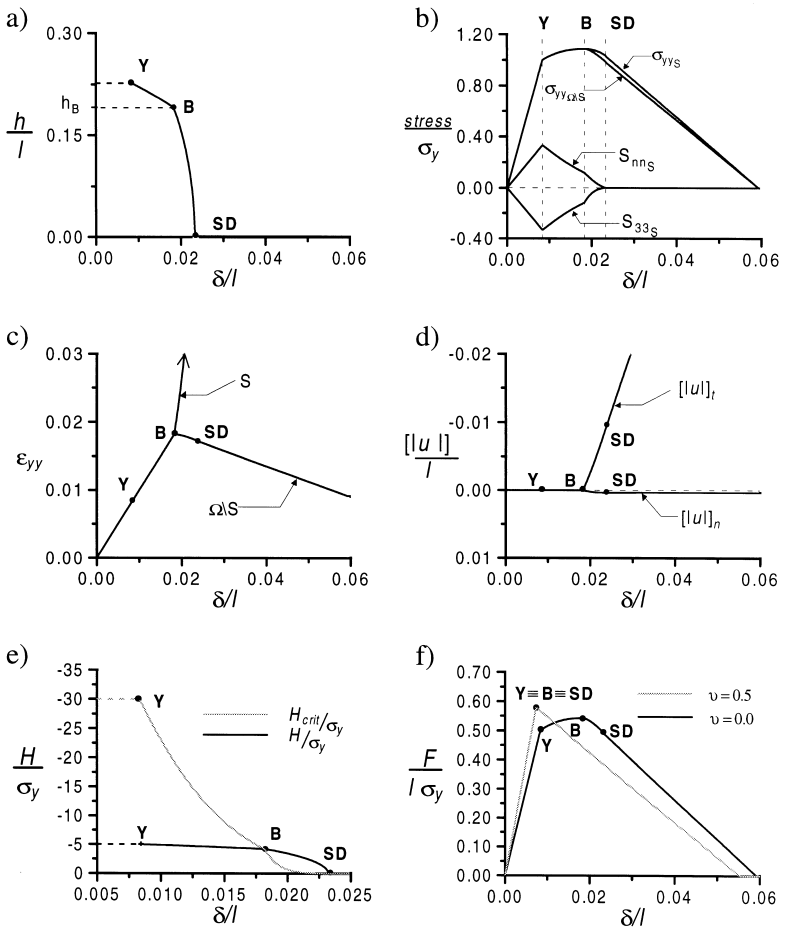

Fig. 6. Uniaxial tension test and J2 plasticity (plane strain). Evolution of some variables.

Figure 6(b) shows the evolution of the vertical component of the stress at the interface, σ_{yy_S}, and outside the interface $\sigma_{yy_{\Omega\setminus S}}$. Notice that they differ beyond the bifurcation point **B**. Also the evolution of the out of plane deviatoric stress S_{33_S} and the normal deviatoric stress S_{nn_S} is shown in that figure. It is worth noting that the *strong discontinuity conditions* $S_{33} = 0$ and $S_{nn} = 0$ coming out from the analysis in Section 6.2.1, are not fulfilled at **B** but, however, they are naturally induced at the onset of the strong discontinuity regime **SD**.

Components of the vertical strain ϵ_{yy_S} and $\epsilon_{yy_{\Omega\setminus S}}$ are plotted in Fig. 6(c). Observe that whereas the strain at the interface ϵ_{yy_S} grows continuously as corresponds to a plastic loading process, the contrary occurs in the rest of the body Ω/S, and the regular strain $\epsilon_{yy_{\Omega\setminus S}} = \bar{\varepsilon}_{yy}$ decreases elastically beyond the bifurcation point **B**. The remaining strain $\epsilon_{yy_{\Omega\setminus S}}$ at the end of the analysis corresponds to the plastic strain generated at the continuous plastic-softening regime (between points **Y** and **B** in the figure).

In Fig. 6(d) evolutions of the normal, $[\![u_n]\!]$, and tangential, $[\![u_t]\!]$, components of the jump are plotted. Observe that there is a slight initial evolution of the normal jump ($[\![\dot{u}_n]\!] \neq 0$) during the weak discontinuity regime, path **B**−**SD** in the figure, but beyond point **SD** the evolution stops as it is predicted by the strong discontinuity analysis [see Eq. $(43)_1$], stating the slip-line character of the induced strong discontinuity.

Figure 6(e) shows the evolution of the computed critical softening parameter $\mathcal{H}_{\text{crit}}$, in accordance to Table 1, and the one of the continuum softening parameter $\mathcal{H}$ emerging from the the values of $\mathcal{H}_y$ and the imposed bandwidth law. Both curves intersect at the bifurcation point **B** where the bifurcation condition $\mathcal{H} \leqslant \mathcal{H}_{\text{crit}}$ is accomplished. Beyond this point the evolution of h determines the evolution of the continuum softening parameter $\mathcal{H}$ according to $\mathcal{H} = h\bar{\mathcal{H}}$. Both curves eventually tend to zero at point **SD** as it is predicted by the theoretical analysis.

Finally, in Fig. 6(f) the load–displacement curves, $F - \delta$, are presented for the two limit values of the Poisson ratio ($\nu = 0$ and $\nu = 0.5$). Observe that the curves are different from each other, since for the very particular case $\nu = 0.5$ yielding, bifurcation and the onset of the strong discontinuity take place simultaneously (points **Y**, **B** and **SD** coincide), and the curve has a straight descending branch. On the contrary, for $\nu = 0$, the paths **Y**−**B** and **B**−**SD**, corresponding to the continuous plastic softening and the weak discontinuity regimes, respectively, are curved and only beyond point **SD** the descending branch is straight. This agrees with the linear character of the discrete constitutive Eq. $(43)_2$ that rules the jump at the interface beyond this point.

Now we consider the same specimen but using a Rankine-type plasticity model as it was described in Section 6.2.2. Since the principal stress σ_1 is vertical, the expected strong discontinuity is an horizontal line for any values of the material properties as it is indicated in Fig. 7(a). This expected result comes out also from the numerical simulation: in Fig. 7(b) the deformed finite element mesh corresponds to a typical mode I split of the bodythrough an horizontal line passing across the element that was initially seeded. The set of elements thatcapture the discontinuity is shown in Fig. 7(c) by the contours of equal total displacement which dark the path crossed by the discontinuity line. In Fig. 7(d) the mode I discontinuity-type is emphasized by the nodal displacement vectors.

Figure 8(a) shows the normal stress vs normal displacement-jump at the discontinuity line, namely, the discrete constitutive Eq. $(47)_1$. In accordance with the theoretical predictions it is a straight line whose slope is characterized by the inverse of the discrete softening parameter $\bar{\mathcal{H}}$. Notice that the yielding point **Y**, the bifurcation point **B**, and the strong discontinuity point **SD** are the same since, for this type of plasticity model, the strong discontinuity conditions Eqs. (33) or (35) are automatically fulfilled at any point of the softening branch as can be checked in Section 6.2.2, Eq. $(44)_2$. Therefore, from Table 1, $\mathcal{H}_{\text{crit}} = 0$ and $h_B = \max\{(\mathcal{H}_{\text{crit}}/\bar{\mathcal{H}}), k\} = k$[15] and the three characteristic points **Y**, **B** and **SD** coincide with each other. In Fig. 8(b) the evolution of both components of the jump in terms of the imposed displacement δ is presented. Observe that the tangential component of the jump $[\![u_t]\!] = 0$ according with Eq. $(47)_2$.

[15] The value of parameter β in Fig. 3(a) does not play here any role, since the bandwidth law is constant ($h = k\ \forall q > q_B$).

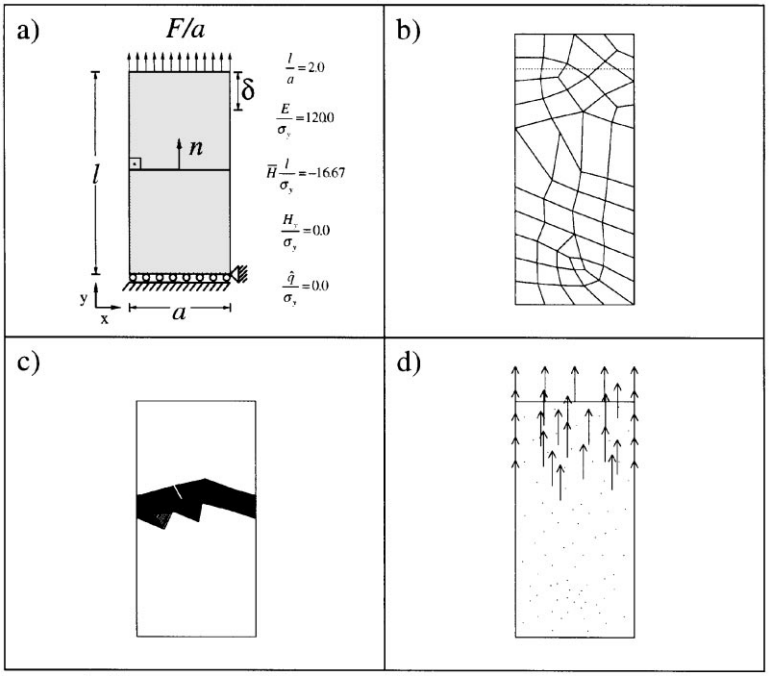

Fig. 7. Uniaxial tension test and Rankine plasticity.

11. Additional numerical simulations

The numerical simulations presented in this Section correspond to the classical geomechanical problem of an undrained soil layer subjected to central or eccentric loading exerted by a rigid and rough surface footing. The same problem was considered in reference (Zienckiewicz et al., 1995), where it was analyzed using an adaptive remeshing strategy to capture the formation of slip lines under perfect plasticity conditions. Here the problem is solved under plane strain conditions and using a J2 plasticity model in the context of the strong discontinuity approach.The bandwidth law is taken linear and such that $\beta = 0.5$. Geometry and results for the two cases analyzed are shown in Figs. 9 and 10. The finite element used in the discretizations is a 6-noded quadratic triangle supplemented with the incompatible displacement referenced to in Section 9. Figure 9 corresponds to the central loading case. Figure 9.2 shows the deformed shape of the finite element mesh at the final stage. In Fig. 9.3 the total displacement contours show the existence of two slips lines that initiate at the bottom corners of the footing and cross each other at a certain point of the symmetry axis. Figure 9.4 shows the displacement vector field. From these it is clear that a triangular wedge of soil beneath the footing moves solidarily with this, vertically downward. This induces the upward movement of two lateral wedges that slide with respect the rest of the soil layer, which remains almost

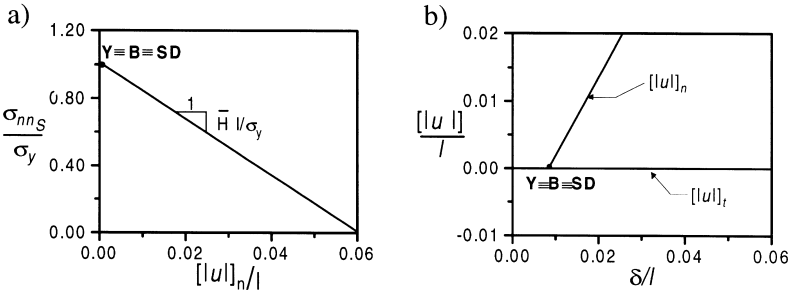

Fig. 8. Uniaxial tension test and Rankine plasticity. Evolution of some variables.

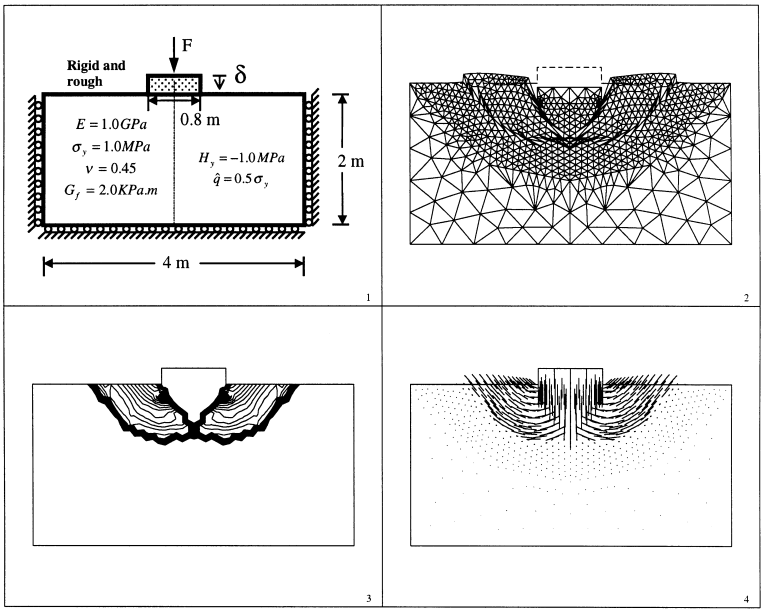

Fig. 9. Numerical simulation of a foundation collapse. Central loading case.

undeformed. The attained solution resembles very closely the classical result obtained using Slip Line Theory (Chen, 1975).

Figure 10 corresponds to the eccentric loading case, the rest of the geometry and properties being the same as previously. Figure 10.2–10.4 show the deformed shape of the finite element mesh, the total displacement contours and the displacement vector field, respectively, at the final stage.The difference with the previous case is obvious. Now, only one strong discontinuity line develops, with a wedge of soil moving side and upward attached to the footing, and sliding with respect to the rest of the layer. The peak load corresponding to the eccentric case is around 25% lower than the one obtained for the symmetric one.

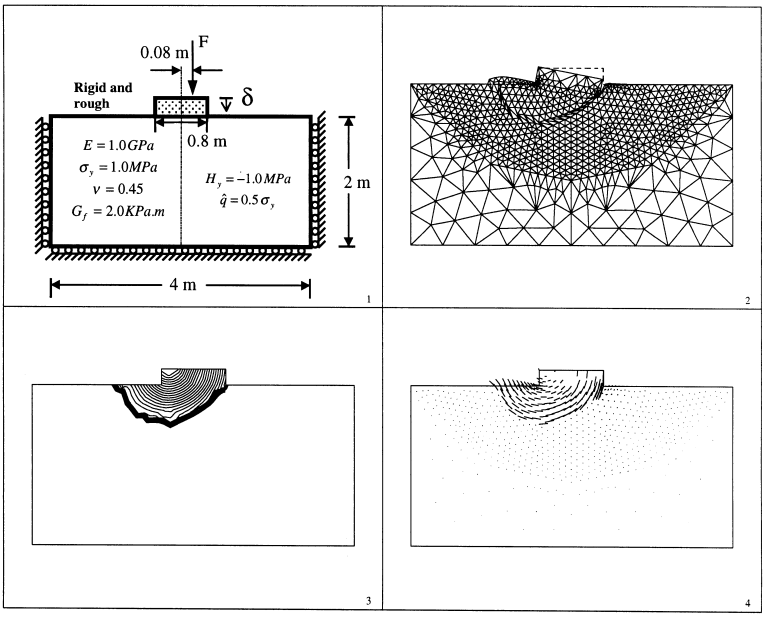

Fig. 10. Numerical simulation of a foundation collapse. Eccentrical loading case.

12. Concluding remarks

Throughout this paper the here called *strong discontinuity approach* to displacement discontinuities induced by continuum stress-strain elastoplastic constitutive equations has been presented. The main features of the approach may be summarized as follows:

- A kinematic state of strong discontinuity, characterized by a discontinuous displacement field across a material discontinuity line, and the corresponding (compatible) unbounded strain field, is considered as the limit case of a regularized kinematic state of weak discontinuity characterized by discontinuous, but bounded strains. These strains intensify across the discontinuity line proportionally to the inverse of the so called *bandwidth* of the weak discontinuity, in such a way that when the bandwidth tends to zero the strong discontinuity kinematic state is recovered. In turn, such a regularized kinematic state of weak discontinuity can be considered representative of a compatible kinematic state of weak discontinuity with continuous displacements and discontinuous strains that intensify (or localize) at a band of the same bandwidth. This provides a first link to the strain localization-type approaches (Ortiz et al., 1987; Needleman, 1988; de Borst et al., 1993; Zienckiewicz et al., 1995) which essentially deal with this type of kinematics. When the bandwidth of the localization band tends to zero the strain-localization state turns to be a strong discontinuity.

- The inception of the discontinuity is characterized through the bifurcation analysis which provides the conditions for the initiation and propagation of such discontinuity. Since the bifurcation analysis lies on the singularity of the localization tensor it provides a second link to the *failure analysis methods* aiming at characterizing the material instabilities in terms of such localization tensor (Runesson et al., 1991; Stein et al., 1995). It is shown that, in general, such a bifurcation can only appear under the form of a weak discontinuity (non-zero bandwidth) and, if strong discontinuities are to be modeled, an additional ingredient is required.
- The variable bandwidth model is then a mechanism devised to induce the strong discontinuity regime from the weak discontinuity one. A bandwidth evolution law, ranging from an initial non-zero value to zero (k-regularized), is postulated as a model property in terms of some stress related variable (here the stress-like variable). Beyond the bifurcation, the continuum hardening/softening parameter is detetrmined as the product of the discrete hardening/softening parameter times that bandwidth, in such a way that a smooth and consistent transition from the weak discontinuity regime to the final strong discontinuity one is obtained.
- The strong discontinuity analysis also provides a very important additional insight on the problem: it is shown that the strong discontinuity kinematics induces from any standard stress-strain constitutive equation a discrete (traction-vector vs displacement-jump) constitutive equation at the interface which is fulfilled once the strong discontinuity regime is reached. This provides an additional link of the approach to the classical non-linear fracture mechanics and the discrete constitutive equation can then be regarded as one of the typical stress-jump constitutive equations used in fracture mechanics to rule the decohesive behavior at the interface (Hillerborg, 1985). The discrete hardening/softening parameter is shown to play an important role in this equations and it can be readily related, in certain cases, to the fracture energy concept.
- A key point of the approach, as it has been presented here, is that the aforementioned discrete constitutive equations are neither derived nor used for practical purposes, but they emerge naturally and consistently from the continuum constitutive equation and the entire simulation can be kept in a standard continumm environment. Therefore, the same continuum constitutive equation rules the continuous and discontinuous regimes of the problem. Although some of such discrete constitutive equations have been derived in the paper as a matter of example, this does not seem in general an easy task for any continumm constitutive equation. Since the proposed approach does not need such derivation it is not restricted at all by that fact. Some representative numerical simulations presented in the paper show that the predicted discrete constitutive laws at the interface are in fact reproduced by the continuum approach.
- The point of stability and uniqueness of the approach has not been addressed here. As far as uniqueness is concerned, in references (Oliver, 1998; Oliver et al., 1998) and for a simple 1D case, the benefits of using the strong discontinuity approach in front of the classical strain localization one were shown and the uniqueness of the solution supplied by the former was proved.

Acknowledgements

The third author wishes to acknowledge the financial support from the Brazilian Council for Scientific and Technological Development-CNPq.

References

Armero, F., Garikipati, K., 1995. Recent advances in the analysis and numerical simulation of strain localization in inelastic solids. In: Owen, D., Onate, E., Hinton, E. (Eds.), Computational Plasticity. Fundamentals and Applications, pp. 547-561.

Armero, F., Garikipati, K., 1996. An analysis of strong discontinuities in multiplicative finite strain plasticity and their relation with the numerical simulation of strain localization in solids. Int. J. Solids and Structures 33(20–22), 2863–2885.

Bazant, Z., Oh, B., 1983. Crack band theory for fracture of concrete. Matériaux et Constructions 93(16), 155–177.

Chakrabarty, J., 1987. Theory of Plasticity. McGraw–Hill, New York.

Chen, J., 1975. Limit analysis and Soil Plasticity. Elsevier.

de Borst, R., Sluys, L. J., Muhlhaus, H. B., Pamin, J., 1993. Fundamental issues in finite element analyses of localization of deformation. Engineering Computations 10, 99–121.

Dvorkin, E., Cuitino, A., Gioia, G., 1990. Finite elements with displacement embedded localization lines intensive to mesh size and distortions. International Journal for Numerical Methods in Engineering 30, 541–564.

Hillerborg, A., 1985. Numerical methods to simulate softening and fracture of concrete. In: Sih, G. C., Di Tomaso, A. (Eds.), Fracture Mechanics of Concrete: Structural Application and Numerical Calculation, pp. 141–170.

Khan, A., Huang, S., 1995. Continuum Theory of Plasticity. John Wiley & Sons.

Larsson, R., Runesson, K., Ottosen, N., 1993. Discontinuous displacement approximation for capturing plastic localization. Int.J. Num. Meth. Eng. 36, 2087–2105.

Larsson, R., Runesson, K., Sature, S., 1996. Embedded localization band in undrained soil based on regularized strong discontinuity theory and finite element analysis. Int. J. Solids and Structures 33(20–22), 3081–3101.

Lee, H., Im., S., Atluri, S., 1995. Strain localization in an orthotropic material with plastic spin. International J. of Plasticity 11(4), 423–450.

Lofti, H., Ching, P., 1995. Embedded representation of fracture in concrete with mixed finite elements. International Journal for Numerical Methods in Engineering 38, 1307–1325.

Lubliner, J., 1990. Plasticity Theory. Macmillan.

Needleman, A., 1988. Material rate dependence and mesh sensitivity in localization problems. Comp. Meth. Appl. Mech. Eng. 67, 69–85.

Needleman, A., Tvergard, V., 1992. Analysis of plastic localization in metals. Appl. Mech. Rev. 45, 3–18.

Oliver, J., 1995a. Continuum modelling of strong discontinuities in solid mechanics. In: Owen, D. R. J., Onate, E., (Eds.), Computational Plasticity. Fundamentals and Applications, vol. 1. Pineridge Press, pp. 455–479.

Oliver, J., 1995b. Continuum modelling of strong discontinuities in solid mechanics using damage models. Computational Mechanics 17(1–2), 49–61.

Oliver, J., 1996a. Modeling strong discontinuities in solid mechanics via strain softening constitutive equations. Part 1: fundamentals. Int. J. Num. Meth. Eng. 39(21), 3575–3600.

Oliver, J., 1996b. Modeling strong discontinuities in solid mechanics via strain softening constitutive equations. Part 2: numerical simulation. Int. J. Num. Meth. Eng. 39(21), 3601–3623.

Oliver, J., 1998. The strong discontinuity approach: an overview. In: Idelsohn, S., Onate, E., Dvorkin, E. N. (Eds.), Computational Mechanics. New Trends and Applications. Proceedings (CD-ROM) of the IV World Congress on Computational Mechanics (WCCM98). CIMNE, pp. 1–19.

Oliver, J., Cervera, M., Manzoli, O., 1997. On the use of J2 plasticity models for the simulation of 2D strong discontinuities in solids. In: Owen, D., Onate, E., Hinton, E. (Eds.), Proc. Int. Conf. on Computational Plasticity, Barcelona, Spain. CIMNE, pp. 38–55.

Oliver, J., Cervera, M., Manzoli, O., 1998. On the use of strain-softening models for the simulation of strong discontinuities in solids. In: de Borst, R., van der Giessen, E. (Eds.), Material Instabilities in Solids, John Wiley & Sons, pp. 107–123 (Chapter 8).

Ortiz, M., Quigley, J., 1991. Adaptive mesh refinement in strain localization problems. Comput. Methods Appl. Mech. Engrg. 90, 781–804.

Ortiz, M., Leroy, Y., Needleman, A., 1987. A finite element method for localized failure analysis. Comp. Meth. Appl. Mech. Eng. 61, 189–214.

Ottosen, N., Runesson, K., 1991. Properties of discontinuous bifurcation solutions in elasto-plasticity. Int. J. Solids and Structures 27(4), 401–421.

Rots, J.G., Nauta, P., Kusters, G.M.A., Blaauwendraad, J., 1985. Smeared crack approach and fracture localization in concrete. Heron 30(1), 1–49.

Runesson, K., Mroz, Z., 1989. A note on nonassociated plastic flow rules. International J. of Plasticity 5, 639–658.

Runesson, K., Ottosen, N.S., Peric, D., 1991. Discontinuous bifurcations of elastic-plastic solutions at phase stress and plane strain. Int. J. of Plasticity 7, 99–121.

Runesson, K., Peric, D., Sture, S., 1996. Effect of pore fluid compressibility on localization in elastic-plastic porous solids under undrained conditions. Int. J. Solids Structures 33(10), 1501–1518.

Simo, J., Oliver, J., 1994. A new approach to the analysis and simulation of strong discontinuities. In: Bazant, Z.B., Bittnar, Z., Jirásek, M., Mazars, J. (Eds.). Fracture and Damage in Quasi-brittle Structures. E & FN Spon, pp. 25–39.

Simo, J., Oliver, J., Armero, F., 1993. An analysis of strong discontinuities induced by strain-softening in rate-independence inelastic solids. Computational Mechanics 12, 277–296.

Stein, E., Steinmann, P., Miehe, C., 1995. Instability phenomena in plasticity: modelling and computation. Computational Mechanics 17, 74–87.

Steinmann, P., Willam, K., 1994. Finite element analysis of elastoplastic discontinuities. Journal of Engineering Mechanics 120, 2428–2442.

Zienckiewicz, O., Huang, M., Pastor, M., 1995. Localization problems in plasticity using finite elements with adaptive remeshing. Int. J. Num. Anal. Meth. Geomech. 19, 127–148.